JOURNAL OF GEOPHYSICAL RESEARCH, VOL. 107, NO. B11, 2300, doi:10.1029/2000JB000050, 2002

Correction published 10 October 2003

Apparent and true polar wander and the geometry of the geomagnetic field over the last 200 Myr

Jean Besse and Vincent Courtillot

Laboratoire de Paléomagnétisme, UMR 7577, Institut de Physique du Globe de Paris, Paris, France

Received 8 November 2000; revised 15 January 2002; accepted 20 January 2002; published 15 November 2002.

[1] We have constructed new apparent polar wander paths (APWPs) for major plates over the last 200 Myr. Updated kinematic models and selected paleomagnetic data allowed us to construct a master APWP. A persistent quadrupole moment on the order of 3% of the dipole over the last 200 Myr is suggested. Paleomagnetic and hot spot APW are compared, and a new determination of ''true polar wander'' (TPW) is derived. Under the hypothesis of fixed Atlantic and Indian hot spots, we confirm that TPW is episodic, with periods of (quasi) standstill alternating with periods of faster TPW (in the Cretaceous). The typical duration of these periods is on the order of a few tens of millions of years with wander rates during fast tracks on the order of 30 to 50 km/Myr. A total TPW of some 30° is suggested for the last 200 Myr. We find no convincing evidence for episodes of superfast TPW such as proposed recently by a number of authors. Comparison over the last 130 Myr of TPW deduced from hot spot tracks and paleomagnetic data in the Indo-Atlantic hemisphere with an independent determination for the Pacific plate supports the idea that, to first order, TPW is a truly global feature of Earth dynamics. Comparison with numerical modeling estimates of TPW shows that all current models still fail to some extent to account for the observed values of TPW velocity and for the succession of standstills and tracks which is observed. *INDEX TERMS:* 1527 Geomagnetism and Paleomagnetism: Paleomagnetism applied to geologic processes; 3040 Marine Geology and Geophysics: Plate tectonics (8150, 8155, 8157, 8158); 8120 Tectonophysics: Dynamics of lithosphere and mantle—general; *KEYWORDS:* Paleomagnetism, polar wander, Earth rotation, TPW

Citation: Besse, J., and V. Courtillot, Apparent and true polar wander and the geometry of the geomagnetic field over the last 200 Myr, *J. Geophys. Res.*, *107*(B11), 2300, doi:10.1029/2000JB000050, 2002.

1. Introduction

[2] Analysis of the fossil magnetization preserved in rocks is the basis for constraining such diverse geophysical problems as dynamo generation in the Earth's core, plate kinematics and paleogeographic reconstructions, and mantle dynamics leading to true polar wander (TPW). The second half of the twentieth century saw the advent and consolidation of plate tectonics: paleomagnetic measurements on lava and sediments coming mostly from continental areas or from hot spot volcanics demonstrated continental drift and could be blended into apparent polar wander paths (APWP); oceanographic exploration led to the discovery of seafloor spreading related magnetic anomalies and transform faults, allowing the construction of kinematic models for each individual ocean basin. APWPs and kinematic models were developed from the '60s to the '80s under the key assumption that, when averaged over a sufficient amount of time, in excess of a few thousand years, the Earth's magnetic field could be described accurately by an axial centered dipole. Of course, both types of largely ocean- and continent-based data could not be independent. Over a decade ago, we proposed [*Besse*, 1986; *Besse and Courtillot*, 1988, 1991, hereinafter referred to as BC91] to blend the two approaches and to use then available paleomagnetic data from North America (NAM), Africa (AFR), Eurasia (EUR) and India (IND) and kinematic models from the Indian, central Atlantic and North Atlantic oceans into a single ''synthetic'' APWP that could next be transferred to any desired plate. On the basis of a selection of 111 poles, the paths were defined in 20 Myr windows extending back to 200 Ma. This first-order analysis provided a reasonable check of the consistency of individual plate paleomagnetic data and kinematic models with the rigid plates and geocentric dipole hypotheses. It also filled gaps in the available APWPs from individual plates. However, the study suffered from a number of limitations in space and time resolution and was not truly global since a number of major plates (South America-SAM, Australia-AUS, Antarctica-ANT and the Pacific-PAC) were not included.

[3] Slight departures from a purely centered dipole field had been noted as early as 1970, when *Wilson* [1970] argued for a far-sided and right-handed distribution of virtual geomagnetic poles during the Cenozoic. A number of analyses confirmed that when averaged over the last few million years, an axial quadrupole component is detectable, with an amplitude on the order of 3 to 6% of the axial dipole [e.g., *Coupland and Van der Voo*, 1980; *Merrill and McElhinny*, 1983;

0148-0227/02/2000JB000050$09.00

Constable and Parker, 1988; *Schneider and Kent*, 1990b; *Quidelleur et al.*, 1994; *Carlut and Courtillot*, 1998; *Johnson and Constable*, 1997]. *Livermore et al.* [1983, 1984] tried to extract such a quadrupolar term in a worldwide paleomagnetic database going back 200 Ma. *Besse and Courtillot* [1991] argued that, for the period prior to 5 Ma going to 200 Ma, a significant quadrupolar term could not be extracted unequivocally from the data available at that time.

[4] On the other hand, comparison of paleomagnetic and hot spot APW led *Besse and Courtillot* [1991] to infer that significant true polar wander, amounting to more than 20°, had occurred in an episodic, irregular way in the last 200 Myr. Recent advances in seismic tomography and dynamic modeling have raised fascinating new questions on the existence and role of slab avalanches, plume events and the viscosity structure of the deep mantle [e.g., *Machetel and Weber*, 1991; *Ricard et al.*, 1993; *Tackley et al.*, 1994; *Steinberger and O'Connell*, 1997; *Bunge et al.*, 1998; *Evans*, 1998; *Richards et al.*, 1999; *Greff-Lefftz*, 2001; M. Greff-Lefftz and P. Bunge, personal communication, 2000] (see, e.g., review by *Tackley* [2000]). Reliable measures of TPW are required to constrain these models.

[5] Paper BC91 was based on a database compiled and updated in our institute [*Besse*, 1986], prior to availability of the global paleomagnetic computerized database of *McElhinny and Lock* [1995]. In its June 1999 version, the GPMD includes all paleomagnetic data published up to the end of 1997. As will be seen below, and still retaining the selection criteria used in BC91, the total amount of reliable data has been increased by a factor of more than 2. Also, significant methodological progress, most notably regarding satellite altimetry data analysis, has led to much improved description of fracture zones and continent/ocean boundaries and hence better reconstructions of past plate motions. Improvement in normalization and correlation of timescales has resulted in data sets such as the Global Seafloor Anomaly Chart [*Royer et al.*, 1992] in which the marine geophysics community has integrated most available data into a single coherent synthesis.

[6] As a consequence of publication of these large sets of new data, we have felt it useful to update our BC91 paper a decade after its publication to try and evaluate whether improved plate reconstructions, APWPs, constraints on field geometry and mantle dynamics could be obtained. In order to decrease the risk of generating artifacts due to limited site distribution [see, e.g., *Quidelleur et al.*, 1994], we have updated the NAM, EUR, AFR and IND data sets and have added data from AUS, ANT, SAM and GRE (Greenland). We have also included some data from ODP/DSDP drilling sites and two skewness poles coming from analyses of marine magnetic anomaly profiles from the Indian Ocean (potential problems when using this type of data are discussed below). This results in much improved geographical coverage both in latitude and longitude (Figure 1). The case of the Pacific plate and data is left to the discussion section.

2. Extended Database

2.1. Paleomagnetic Data From Continents

[7] Faster paleomagnetic data search and treatment is now made easy due to the availability of the computerized Global Paleomagnetic Database (GPMD) of *McElhinny and Lock* [1995]. We have used the June 1999 version (GPMD V3.3). In the process of using and searching the database, we have uncovered a few errors and inconsistencies. The more frequent occurrences were older data later re-used in a larger study or an update without any notice of this redundancy in the database. In order to avoid confusion in the database, and to allow others to easily check our computations, we have preferred not to alter the database version we started with, but rather send a list of the problems to the managers of the database for future revisions, equally accessible to all. We have, however, checked that these errors and inconsistencies were sufficiently few and small that their integration in the master APWPs resulted in changes of mean pole positions always less than 1°, or in mean age less than 1 Myr. As a result, these changes would hardly alter the Figures.

[8] The key question is which selection criteria are applied to sift the base and extract a robust high quality subset that allows one to address a given problem. As was already the case in BC91, we have decided to retain data from both magmatic and sedimentary rocks. In a similar recent study of TPW, *Prévot et al.* [2000] chose to retain only magmatic rocks, which they believe to carry a more reliable magnetization, namely a thermoremanent magnetization (TRM). The question of the relative reliabilities of sedimentary and volcanic magnetizations is an old one in paleomagnetism. For instance, deepwater sediments can have significant compaction errors [e.g., *Celaya and Clement*, 1988; *Tarduno*, 1990] but there are none in our data set. We believe that there can be as many problems with volcanic rocks as with sediments (e.g., remagnetizations versus inclination shallowing, too short versus too long integration time for recording of magnetization) and in any case it is interesting to compare results obtained in either case, as will be done below.

[9] For the sake of comparison, and because we believe the end result to be sufficiently reliable, we have retained a selection procedure similar to BC91. Applying selection criteria automatically, i.e., writing selection filters, is quite straightforward with a properly computerized database. The BC91 criteria were the following: (1) at least 6 sites and 36 samples per study; (2) a 95% confidence interval less than 10° in the Cenozoic and 15° in the Mesozoic; (3) evidence for successful alternating field and/or thermal demagnetization (i.e., Demagnetization Code equal to or larger than 2 in the *McElhinny and Lock* [1995] terminology); (4) dating uncertainties less than 15 Myr; and (5) absence of remagnetization ensured by the fact that differences between magnetization and stratigraphic ages should be less than 5 Myr and by rejecting poles with a negative fold test or negative reversal test.

[10] These simple criteria are of course to a large degree arbitrary and are based on our experience in trying to eliminate most problematic studies. This is discussed in BC91 and compared to different selection criteria used by other authors. Part of the justification comes a posteriori from a comparative examination of the results.

[11] One of the key aspects of our selection process has been an attempt to identify mobile zones from which data should be excluded from what should in principle be rigid plates. This is important not only for plate reconstructions, but also for field geometry analysis: *Carlut and Courtillot*

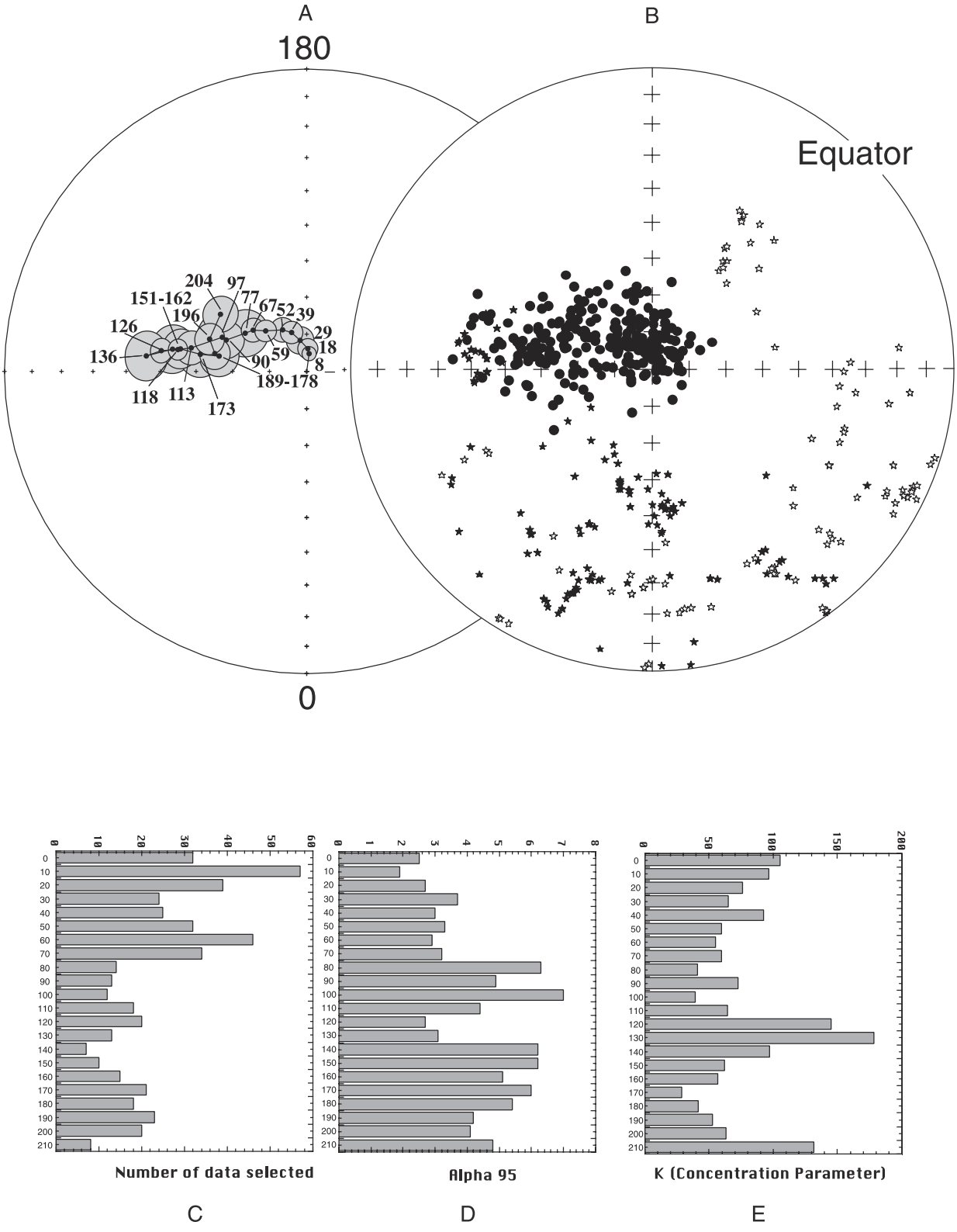

Figure 1. (a) Master apparent polar wander path for Africa from the Present back to 200 Ma, with associated ellipses of 95% confidence in shaded gray (averages every 10 Myr, with a 20 Myr sliding window); actual mean ages for each time window are indicated. (b) Distribution of individual paleomagnetic poles and sampling sites; dots: all poles used in this study to construct the master APWP, transferred to South African coordinates according to their age; stars: site locations reconstructed to appropriate time in South African frame (solid star, Northern Hemisphere, open star, Southern Hemisphere). Histograms from the Present back to 200 Ma for (c) number of data, (d) confidence intervals at the 95% level, and (e) Fisher's concentration parameter K.

[1998] noted, for instance, in a study of the mean geomagnetic field over the last 5 Myr that inclusion of tectonically rotated Ethiopian data produced a very erroneous mean field model. Some tectonic areas, such as mountain ranges (Himalayas, Alpine ranges) or rift zones (Afar in Africa), are of course rather obvious and sites from these regions were eliminated. Others zones, such as the Colorado plateau in North America or the African rift south of the Afar depression are less straightforward. And actually, rocks often outcrop simply because of some amount of tectonic deformation. Our task is then to test whether the extent of deformation requires that the data be rejected or not. A major source of error is linked to local tectonic rotations about vertical axes: crustal deformation at a large scale or at depth may lead to small block rotations and many paleomagnetic studies fail to take into account the plunge of fold axes (the resulting error may exceed 15°). Detailed analysis of individual poles and comparison with synthesized APWPs may allow one to spot remaining outliers with a previously undetected tectonic origin. In some cases, we have used another method: some poles that where suspected to have undergone rotations without significant poleward motion have been integrated using a method derived from *McFadden and McElhinny* [1988]. We treated these poles using only inclination data, i.e., as small circle constraints, as we also did for data coming from DSDP Legs (see below). These poles (11 studies in western North America, one in South America and one in Europe) are marked in Table 1.

[12] Another major problem is to determine to what extent large plates, such as Eurasia or Africa, can be considered as rigid. The ocean-based kinematic syntheses of *Müller et al.* [1993] imply that Africa and South America need to be subdivided into a small number of rigid subplates that have undergone some (slight) amount of differential rotation since the time of breakup. Recent surveys of South Asian data [*Cogné et al.*, 1999; *Yang and Besse*, 2001] have emphasized differences between the Cretaceous segment of the Chinese APWP and the synthesized APWP of BC91 for Eurasia at the same period. *Cogné et al.* [1999] concluded that ''rigid'' Eurasia may have actually undergone some amount of internal deformation, possibly due to the relative motions of three rigid subplates. Therefore, and contrary to our analysis in BC91 where China was assumed to have been rigidly attached to Eurasia (hence Europe) since the Cretaceous, we have excluded Chinese data from the present compilation. This final data set comprises 221 poles (Tables 1a–1g).

2.2. Oceanic Data

2.2.1. Data From Skewness of Marine Magnetic Anomalies

[13] The skewness of a (usually marine) magnetic anomaly is the phase shift required to restore the shape of the measured anomaly to the one which would have been observed, had the anomaly been created at the geomagnetic pole [*Schouten and McCamy*, 1972]. The anomaly is then ''undistorted'', i.e., has the same symmetry elements as the magnetic source body. This is particularly useful for accurate determination of the location of the center or edges of individual crustal blocks corresponding to a given chron. The value of skewness depends on the inclination and declination of the original remanence of the block, on the present field direction (inclination and declination) and on the azimuth of the magnetized body (i.e., generally of the ridge where the crustal block was generated). A great circle of possible pole positions is deduced from the skewness value in the hypothesis of a dipolar centered geomagnetic field. The intersections of a set of such semicircles derived from the same anomaly (chron) at distant locations on the same plate in principle allow the determination of a virtual geomagnetic pole [e.g., *Schouten and Cande*, 1976; *Gordon and Cox*, 1980].

[14] The analysis of the skewness of marine magnetic anomalies generated by seafloor spreading is therefore a way of obtaining pole positions for oceanic plates, for which other kinds of data may be lacking. The method has been extensively applied by R. Gordon and colleagues [e.g., *Petronotis and Gordon*, 1999] to the case of the Pacific plate. Because of problems in connecting that plate to the others through a plate circuit, we have not included it in the set used for construction of synthesized APWPs; we return to this question in the final section of this paper. We note, however, that the theoretical potential of the skewness method for the determination of VGPs from purely oceanic plates is unfortunately hampered by strong limitations due to the parasitic effect of neighboring sources and/or to the tectonic tilt of blocks generated close to the spreading center, leading to strong artifacts: *Cande* [1976] discusses the problems of ''anomalous skewness'', which are further elaborated on by *Petronotis et al.* [1992] and *Dyment et al.* [1994].

[15] In the case of the Indian Ocean, careful analysis [*Dyment et al.*, 1994] of conjugate marine magnetic anomalies from the Carlsberg ridge and the Wharton Basin, and the Central and South-East Indian ridges, leads to the conclusion that anomalous skewness becomes negligible when the spreading rate is faster than 50 km/Myr. The determination of skewness from anomaly 34 (84 Ma), i.e., the time when India began its northward motion, up to anomaly 21 (47 Ma), when a sudden velocity drop resulted from the India-Asia collision [*Patriat and Achache*, 1984] is possible because the spreading rate is far above this critical value. *Dyment et al.* [1994] found that anomalies 21, 24 and 29 were suitable for the determination of reasonably accurate paleolatitudes; they found good agreement between the great circle of possible pole positions for these anomalies and the BC91 APWP.

[16] However, *Dyment et al.* [1994] did not publish such great circles for anomalies 25 and 26 which are prominent in the Indian Ocean. *Torcq* [1997] and F. Torcq and J. Besse (manuscript in preparation, 2002) filled this gap, by analyzing profiles from the Somali, Madagascar, Arabia, Crozet, and Central Indian basins. Anomalies 25 and 26 (61.5–57.2 Ma following the *Harland et al.* [1989] timescale) are easy to recognize and their shapes are well determined. Anticipating results given later in this paper, the intersections of skewness derived circles for the Indian and African plates yield a pole in excellent agreement with data from other continents. There are unfortunately no other sets of usable skewness data from the plates involved in our synthesis.

2.2.2. Oceanic Data From Boreholes

[17] Paleolatitudes can also be inferred from inclination measurements performed on unoriented cores [e.g., *Cox and*

Table 1a. Selected Paleomagnetic Data for Antarctica Used in This Study Extracted From the GPMD V3.3 Database[a]

Rock Name	Age	Dage	Plat	Plong	*Dp*	*Dm*	Slat	Slong	*B*	*N*	Dc	Tests	Rock Type	RNO	Year
McMurdo Volcanics	1.5	3	86.4	81.2	13.4	13.7	−77.5	161	14	212	3	Ro	extrusives	1187	1983
McMurdo Volcanics	2	4	87.3	317.3	6.3	6.3	−78	165.4	47	450	3	Rc	extrusives	398	1988
Pensacola Mountains, Dufek Intrusion	172	8	60	43	10.3	11.5	−82.6	−50	30	91	2	Rb	intrusives, gabbro	2489	1972
Nash Hills-Pagano Nunatek Intrusives	175	16	41.2	55.2	5.3	5.3	−82.8	−88.6	8	37	4	Rc	intrusives, granite, baked sediments	1107	1987
Northern Prince Albert Mountains, Ferrar dolerites	177	3	47.8	45.5	5.5	5.5	−74.5	162	15	227	3	M	intrusives, dolerites	7079	1993
Northern Prince Albert Mountains, Ferrar dolerites	177	3	78.8	0.9	5.9	5.9	−75.4	161.3	7	98	3	M	intrusives, dolerites	7080	1993
Northern Prince Albert Mountains, Ferrar dolerites	177	3	45	40	3	4	−78	162	46	83	2	Co, M	intrusives, dolerites	3592	1962
Queen Alexandra Range, Mount Falla Lavas	193	30	52	24.1	6.8	7.7	−84	165	14	84	2	M	extrusives	3231	1971
Queen Alexandra Range, Jurassic Intrusions	193	30	52.5	23.9	8.4	9.5	−84	165	7	42	2	M	intrusives	3232	1971
Queen Alexandra Range, Storm Peak Lavas	193	30	44.1	51.5	8.8	11	−84	165	12	72	2	M	extrusives	3230	1971

[a] From *McElhinny and Lock* [1995]. Column headings are rock name, where sampled, formation or unit; age, mean age of magnetization, in Ma; Dage: maximum age of magnetization minus minimum age (i.e., error is Dage/2); Plat, Plong, VGP latitude (°N) and longitude (°E); *Dp*, *Dm*, semiaxes of the 95% level confidence ellipse (in degrees) for the VGP; Slat, Slong, site latitude and longitude; *B*, number of sites; *N*, number of samples; Dc, demagnetization code, or quality; tests, N, no test; M, rock magnetic test; G, F, R, conglomerate, fold, and reversal tests, respectively; O, a,b, c, +, significance level of tests; RNO, reference number in the GPMD; year, year of publication.

Table 1b. Selected Paleomagnetic Data for India Used in This Study Extracted From the GPMD V3.3 Database[a]

Rock Name	Age	Dage	Plat	Plong	*Dp*	*Dm*	Slat	Slong	*B*	*N*	Dc	Tests	Rock Type	RNO	Year
Sonhat Sill	61.5	7	37	285	2.1	3.2	23	82	11	62	3	N	intrusives, dolerite	2892	1974
Deccan Traps, 11 sections combined	62.5	5	34.3	261.4	3.9	3.9	18.5	76.5	181	1070	3	Ro	extrusives, basalts	2874	1973
Deccan Traps, Jabalpur	62.5	5	48	286	3	6	23.1	80.8	8	93	2	N	extrusives, basalts	2915	1971
Deccan Traps, Aurangabad	62.5	5	33	287	5	7.3	19.8	76.5	25	142	3	N	extrusives	2967	1972
Mt. Pavagarh Traps	64	8	39.2	285.6	4	6.8	22.5	73.5	16	88	3	N	extrusives, basalts, rhyolites	2755	1974
Deccan dike swarms	65.5	5	37.2	280.5	9.7	9.7	21.5	74.3	11	67	3	Rc	intrusives, dolerites	8106	1996
Deccan Traps–Nagpur to Bombay traverse	65.5	5	38.4	282.4	6.1	6.1	20	75	16	119	4	Rc	extrusives, basalts	5727	1991
Deccan Traps, Malwa Plateau	65.5	5	36.3	270.4	11.4	17.4	22.5	75.8	13	76	2	Rb	extrusives, basalts	2975	1971
Deccan Traps, Mahabaleshwar	65.5	5	40	276	7.4	7.4	17.9	73.6	28	190	2	Rc, M	extrusives, basalts	2693	1972
Deccan traps, Dhar region	65.5	5	29	293	5.3	8.3	22.4	75.4	6	37	3	Rc, M	extrusives	67	1981
Deccan Traps	66	4	32.6	290.8	3.8	5.9	20	76.5	21	110	4	Rc, M	extrusives, basalts	564	1986
Central Kerala dikes	69	2	34.6	274	11.8	15.5	9.7	76.7	6	39	3	Ro	intrusives, dolerites	7150	1994
Rajmahal Traps combined	116	2	7.5	296.5	3	3.5	24.5	87.5	48	294	3	Ro	extrusives, basalts	3000	1971

[a] See Table 1a footnote.

Table 1c. Selected Paleomagnetic Data for Australia Used in This Study Extracted From the GPMD V3.3 Database[a]

Rock Name	Age	Dage	Plat	Plong	*Dp*	*Dm*	Slat	Slong	*B*	*N*	Dc	Tests	Rock Type	RNO	Year
Newer Volcanics	2.5	5	86.6	266.3	1.9	1.9	−38.5	143.5	46	133	2	Ra	extrusives	1897	1971
Port Campbell Limestone, Glenample Formation	12	4	77.2	303.5	4.2	4.2	−38.7	143.1	30	48	3	N	sediments, limestone	139	1985
Springfield Basin, red clays	14	18	80.4	270.5	8.4	8.4	−32.5	138.5	6	37	2	Rc	sediments, red clays	1976	1976
New South Wales, Nandewar, Warrumbungle Volcanoes	17.5	5	79.4	246	4.2	4.2	−32	150	51	149	2	Ro	extrusives, basalts	1924	1974
Tweed and Main Range Volcanos combined	22.5	5	77.4	290.9	4.1	4.1	−30	150	75	278	2	Ro	extrusives, basalts	1925	1974
Queensland, lavas and dikes	23.5	3	78	260	8	12	−27	152.2	12	68	3	Rc	extrusives, intrusives	1858	1966
Liverpool, Springsure Volcanoes and older volcanics combined	30	10	68.9	272.4	4.3	4.3	−35	150	52	162	2	Ro	extrusives, basalts	1926	1974
Victoria, Browns Creek Formation	37	4	65.5	292.5	2.5	2.5	−38.8	143.4	33	66	4	Rb, M	sediments, red-brown clays	7097	1994
Barrington Volcano, Nerriga Province, older volcanics combined	50	20	68.5	310.9	5.2	5.2	−35	150	46	143	2	Ro	extrusives, basalts	1927	1974
SW Queensland, Morney Profile, Eromanga Basin	50	30	58.8	298	3.8	3.8	−27	141.5		37	2	Rb	sediments, weathered	1972	1978
Sydney Basin, Mogo Hill Basalt	57.5	3	40.6	310.2	8.6	8.6	−33.2	151.1	9	44	3	M	extrusives	241	1981
New England, New South Wales, weathered profile	60	20	59.2	297.2	9.1	9.9	−30.5	151.5	7	53	4	Ro	sediments, weathered	1964	1988
Mt. Dromedary Intrusive Complex	95	10	56	318	9	9	−36.3	150	22	55	3	Co, M	intrusives	1848	1963
Western Australia, Bunbury Basalt	97.5	15	49	341	10	10	−33.4	115.6	5	54	2	Ro, M	extrusives, basalts	1932	1976
Tasmania, Cygnet Alkaline Complex	105	10	50	338	10	10	−43	147	15	45	2	Co	intrusives, alkali-syenite	1973	1962
Sydney Basin, Prospect dolerite	168	10	53	359.6	6.4	6.4	−33.8	150.9	10	59	4	N	intrusives, dolerite	84	1982
Tasmanian Dolerite	174	16	50.7	354.5	5.2	5.2	−42	147.5	21	42	2	N	intrusives, dolerite	1960	1977
New South Wales, Garrawilla Volcanics and Noombi extrusives	197	20	46.1	355.2	10	10	−31	150	14	36	2	N	extrusives	1938	1976

[a] See Table 1a footnote.

Table 1d. Selected Paleomagnetic Data for South America Used in This Study Extracted From the GPMD V3.3 Database[a]

Rock Name	Age	Dage	Plat	Plong	*Dp*	*Dm*	Slat	Slong	*B*	*N*	Dc	Tests	Rock Type	RN-O	Year
Fernando de Noronha Volcanics, Brazil	2.5	2.5	87	164.8	3.3	6.4	−3.8	−32.4	22	88	2	Rc	extrusives, intrusives	3400	1967
Basalts, Quixaba Formation, Brazil	3.5	1.5	80.3	234	2.9	2.9	−3.9	−32.4	7	61	3	M	extrusives, basalts	553	1986
Lipiyoc Formation, Argentina[b]	8.5	1	85.7	260.5	7.9	7.9	−22.5	−66.5	17	159	4	Ro, M	extrusives, ignimbrites	7818	1996
Remedios, Sao Jose Formations, Brazil	9.5	1.5	84.5	136	7.5	7.5	−3.9	−32.4	7	45	3	Ro, M	extrusives, basalts	555	1986
Rio Azul Sediments, Argentina	11	4	80.2	76	2.8	4.7	−30.7	−68.8	89	267	3	Rb	sediments	8129	1990
Neuquen-Mendoza Lavas, Argentina	14	28	87.3	165.9	9.7	10.4	−37.5	−70	22	198	2	Rc, M	extrusives, basalts	3319	1968
Miocene Basalt, Argentina	16.5	23	85.8	179.1	10.9	14.8	−37.5	−70	6	42	3	Ro, M	extrusives, basalts	3145	1970
Volcanic Hills, Argentina	75.5	19	70.2	224.5	12.2	12.2	−33	−65	12	36	3	Ro	extrusives, basalts	94	1983
Intrusives, Cabo de Santo Agostinho, Brazil	92	14	87.6	135.1	4.5	4.5	−8.4	−35	9	100	2	N	intrusives	651	1980
Volcanics and red beds, Sierra de Los Condores, Argentina	111	28	84.2	270.6	4.7	4.7	−32.2	−64.1	8	78	2	Co	extrusives, sediments, redbeds	2238	1976
Maranhao Basin Intrusives, Brazil	118	12	83.6	261	1.9	1.9	−6.5	−42	21	190	2	N	intrusives	611	1979
Cerro Barcino Formation, Argentina	119	13	84.9	0.8	5.6	5.6	−43.5	−69	11	66	4	F+	sediments, sandstones, siltstones	7498	1994
Serra Geral Basalts, Brazil	119	10	84.6	295.4	3.7	3.7	−29	−50	37	260	2	Rb	extrusives, basalts	2387	1976
Serra Geral Formation, Brazil	119	10	78.2	234.1	5.7	5.7	−26	−53	30	74	2	Rc, Co, M	extrusives, basalts, intrusives, diabases	3599	1962
Vulcanitas Cerro Colorado Formation Argentina	121	12	81	194	13.4	13.4	−32	−64	6	86	2	N	extrusives, intrusives, sediments, redbeds	2700	1972
El Salto-Almafuerte Lavas, Argentina	124	10	72	205	6.5	6.5	−32.2	−64.2	15	65	2	Rc	extrusives	2003	1978
Serra Geral Formation, Brazil	128	15	83.5	280.5	2.2	3.6	−29	−50	79	261	2	Rb	extrusives, basalts, andesites, rhyolites	7675	1983
Serra Geral Formation Younger Group, Brazil, Uruguay	131	8	82	218	7.8	7.8	−26	−52	28	85	3	Ro, M	extrusives, basalts	6280	1990
Serra Geral Formation Main Group, Brazil, Uruguay	136	7	85	288	1.1	1.1	−26	−52	287	850	3	Ro, M	extrusives, basalts	6279	1990
Maranhao Basalts, Brazil	175	4	85.3	82.5	6.9	6.9	−6.4	−47.4	15	121	2	N	extrusives, basalts	610	1979

[a] See Table 1a footnote.
[b] Declinations are suspect, due to possible local tectonic rotations, and inclinations only are used (see text).

Table 1e. Selected Paleomagnetic Data for Africa Used in This Study Extracted From the GPMD V3.3 Database[a]

Rock Name	Age	Dage	Plat	Plong	*Dp*	*Dm*	Slat	Slong	*B*	*N*	Dc	Tests	Rock Type	RNO	Year
Kenya and Tanzania, East African Volcanics	1	2	88.7	104	3.2	3.2	0	36	54	155	2	Rc, M	extrusives	2234	1976
Libya, Haruj Assuad Volcanics	1	2	83	171	5	8.5	27.8	17.3	14	78	2	Rc	extrusives, basalts	2611	1974
Northern Nigeria, Jos Plateau newer basalts	1	2	66.9	242.2	2.4	4.8	9.6	8.8	10	97	3	Rb	extrusives, basalts	6134	1991
Canary Islands, Gran Canaria and Tenerife basalts	1	1	80.2	140	3	5.2	28.1	−16.5	11	43	2	N	extrusives, basalts	2097	1978
Madagascar, Volcanics, Itasy	1	2	77.7	267.2	9.3	14.5	−19.1	46.7	8	56	2	N	extrusives	2330	1971
Sao Tome Volcanics	2	2	86.4	199.4	2.4	4.8	0	6.5	49	164	2	Rc	extrusives, basalts	2509	1972
Tanzania, Ngorongoro Caldera	2.5	1	81	62	6	12	−3.2	35.5	20	102	2	Ro, M	extrusives	2944	1971
Combined Gran Canaria and Tenerife younger basalts	2.5	2.5	82.9	131.9	2.4	4.1	28.1	−16.5	24	128	2	Ro	extrusives	2099	1978
Madagascar, Plio-Pleistocene Volcanics combined	2.5	5	82.9	255.5	4	6.6	−16.5	47.6	28	171	2	Rc	extrusives	2329	1971
Kenya and Tanzania, East African Volcanics	3.5	3	86.5	147.6	2.3	2.3	0	36	102	255	2	Rb, M	extrusives	2235	1976
Spain, Canary Islands, Late Tertiary basalts	3.5	1.5	83.8	126.8	3.8	6.3	28.1	−16.5	13	85	2	Ro	extrusives	2098	1978
Pliocene Volcanics, Canary Islands and Madeira	3.5	1.5	82.6	128.8	3.2	3.2	28	−16	72	214	2	Rb, M	extrusives, basalts	2517	1973
Volcanics, Kenya	4	6	83.9	296.6	3.9	3.9	−1.5	36	161	240	2	Ro	extrusives, basalts, welded tuff	796	1979
Spain, Lanzarote, Canary Islands, Famara Volcanics	7.5	2.5	87.5	178.2	5.4	8.5	29.2	−13.5	17	108	4	M	extrusives, basalts	7644	1995
Canary Islands, Basalts Series II, Fuerteventura	8	6	77.8	146.2	3.2	5.8	28.6	−14.1	10	51	3	N	extrusives	756	1979
Kenya, Ngorora Formation	11.5	3	85.7	255.8	1.9	3.8	1	35.5	104	312	4	Rb	sediments	8133	1990
Libya Volcanics, Jebel Soda	11.5	3	78.4	196.1	7.4	7.4	28.7	15.6	12	138	2	Rc	extrusives, basalts	2521	1973
Libya Volcanics, Jebel Soda	11.5	3	69	184	6.8	6.8	28.8	15.5	9	57	2	Ro	extrusives, alkali basalts	2625	1975
Kenya and Tanzania, East African Volcanics	12	2	86.5	186.6	6.1	6.1	0	36	22	161	2	Rc	extrusives	2236	1976
Miocene Volcanics, Canary Islands	13	8	81.9	114.4	3.5	3.5	28	−16	99	291	2	Rb, M	extrusives, basalts	2519	1973
Volcanics, Kenya	13.5	3	80.1	34.2	8.9	8.9	−1.6	35.9	14	56	2	N	extrusives, nephelinites, welded tuff.	797	1979
Santa Antao Volcanics, Cape Verde	14	9	84.5	168.2	3.7	6.9	17.1	−25.1	40	120	2	Rc	extrusives, intrusives	3263	1968
Sao Nicolau Volcanics, Cape Verde	14	9	86.8	124.7	4.2	7.8	16.6	−24.3	12	36	2	Ro	extrusives	3265	1968
Sao Tiago Volcanics, Cape Verde	14	9	82.3	178.9	2.8	5.3	15.1	−23.6	30	93	2	Rc	extrusives, intrusives	3268	1968
Sao Vicente Volcanics, Cape Verde	14	9	83	87.1	3.7	6.9	16.8	−25	46	143	2	Rc	extrusives, intrusives	3264	1968
Kenya, Turkana lavas	18.5	9	84.6	163.3	2.3	2.3	0	36	62	109	2	Rb, M	extrusives	2237	1976
Algeria, Massif de Cavallo	19	6	86.8	22.9	2.2	3.3	32	5	13	51	2	N	extrusives	2791	1969
Egypt, Cairo region basalts	19.5	7	66	167	2.3	2.3	30	31	11	132	4	F+	extrusives, basalts	8110	1995
Egypt, Cairo region basalts	19.5	7	76	111	3	3	30	31	18	216	4	F+	extrusives, basalts	8111	1995
Principe Volcanics	24	4	82.8	96.6	4.5	9	1.5	7.5	25	78	2	Rc	extrusives, basalts	2512	1972
Ethiopian Traps, Lima Limo	30	1	75.5	207.5	3.5	6.9	13.2	37.9	20	302	4	Rc	extrusives, basalts	6691	1999
Ethiopian Traps, Wegel Tena	30	1	81.1	226.4	4.3	8.6	11.5	39.2	20	158	4	Rc	extrusives, basalts	6691	1999
Ethiopia Southern Plateau Volcanics	34	8	75.1	170.3	6.4	6.4	9.1	41	22	92	2	Rc	extrusives	2764	1974
Egypt, Iron ores combined, Baharia Oasis	37	4	83.5	138.6	7	7	28.2	28.9	9	109	3	Ro	sediments, iron ores	769	1981
Egypt, Basalts, Wadi Abu Tereifiya	44.5	11	69.4	189.4	3.2	6.1	30	32.1	6	111	3	N	extrusives, basalt	1	1979
Ethiopian Trap Series	50	30	80.8	167.7	4.3	4.3	9.3	39	20	52	2	Ro	extrusives, basalts	3025	1970
Egypt, Nubian Sandstone Combined	72.5	15	81.8	222.7	3.3	3.3	24.5	33.5	23	255	3	Rb	sediments, sandstones	766	1981
Madagascar, Volcanics Combined	74	12	63.5	219.6	4.1	4.1	−21	47.3	30	211	2	N	extrusives	2338	1971
Sudan, Northern Volcanic Field	80.5	5	55.9	277.8	11.3	11.3	19	33.3	6	54	3	M	extrusives, basalts, latites, phonolites	1179	1989
Madagascar, Volcanics, Massif d'Androy	82	16	65	252	8	8	−24.3	46	7	36	2	N	extrusives	2789	1969
Madagascar, Volcanics Combined	89.5	3	69.1	240.1	4.9	4.9	−19	44.9	33	170	2	N	extrusives	2339	1971
South Africa, Cretaceous Kimberlites 1	90.5	19	64.1	226.1	5.2	5.2	−29	26	14	118	4	M	intrusives, kimberlite	5983	1989
Egypt, Wadi Natash Volcanics	93	14	69.3	258.1	5.8	5.8	24.4	34.3	15	342	3	N	extrusives, basalts, andesites	765	1981
Mozambique, Lupata Series Volcanics	111	4	61.8	259.5	3.2	4.5	−16.7	34.2	7	61	2	F+	extrusives, trachytes, phonolites, kenyites	3586	1963
Namibia, Kaoko lavas	122	19	48.3	266.6	2.5	3.9	−20	14	40	118	3	Ro, M	extrusives, basalts	2580	1975
Zimbabwe, Mateke Hills Complexes	173	8	58.7	260.5	7	9.4	−21.8	31.2	6	49	3	N	intrusives, granite, granophyre, gabbro	3452	1964

[a] See Table 1a footnote for explanation.

Table 1f. Selected Paleomagnetic Data for Europe Used in This Study Extracted From the GPMD V3.3 Database[a]

Rock Name	Age	Dage	Plat	Plong	*Dp*	*Dm*	Slat	Slong	*B*	*N*	Dc	Tests	Rock Type	RNO	Year
River Volga Sediments	1	2	81	227	4.3	5.9	47	47	8	67	2	M	sediments, clays, sandstones	3883	1979
Massif Central Lavas 2	3	4	77.5	187.5	12	12	44.6	3.5	10	73	3	Rc	extrusives, basalts	3055	1970
Coiron Lavas	6	10	80.4	142.9	7.2	7.2	45	4	36	220	2	Ro	extrusives, basalts	3050	1970
Suevites, Nordlinger Ries	15	2	77.5	146.3	1.6	2.1	49.9	10.5	12	111	2	N	metamorphics, tuffaceous rocks	3472	1965
Vogelsberg Volcanics	16.5	3	85.1	200.9	6.6	8.3	50.5	9.4	31	93	4	Rc, M	extrusives, basalts	6264	1990
Rheinland Pflaz Volcanics	22.5	13	70	108	6	8	50.5	7.5	22	53	2	Ro	extrusives, basalts, trachyte, phonolite	3603	1962
Lausitz Volcanics	22.5	13	74.6	120.5	6.5	8.2	51	14.7	24	148	2	Rc, M	extrusives, basalts, phonolites	3304	1967
Tertiary Volcanics, northern Bavaria	28.5	25	78	140	7.2	7.2	50.1	11.4	22	316	2	Rc, M	extrusives	2287	1977
Hocheifel Tertiary Volcanics	34	22	80.8	182	4.2	4.2	50.3	7	47	351	3	Rb	extrusives, andesites, basalts	781	1984
Scottish Tertiary dikes	46.5	23	73.4	196.8	4	5	55	−4	21	84	2	Ro, Co	intrusives, dykes	3456	1966
Tertiary dikes	53	6	77	213.5	10.9	14.2	53.6	−2.9	11	54	2	Co	intrusives	3182	1969
Faeroe Island Volcanics	57	3	77	161	2	2	62	−7	253	1809	2	Ro	extrusives	3208	1970
Northern Ireland, Antrim Basalts	57.5	15	69.6	162.9	5	7	55	−6	25	225	2	Co	extrusives, basalts	3026	1970
Northern England, Skye Lavas	57.5	15	71.5	165.2	2.8	3.8	57.4	−6.3	90	344	2	N	extrusives, basalts	2506	1972
Northern England, Cleveland-Armathwaite dike	58.5	13	75	240	5.5	5.5	54.5	−2	10	83	3	Co	intrusives	2870	1974
U.K., Rhum and Canna igneous rocks	59	2	81.4	181.9	3.2	3.9	57	−6.5	109	453	2	Rc, M	extrusives, intrusives, dykes	68	1981
Scotland, dike swarm, Skye	59	2	82.5	158	2.1	2.5	57.1	−5.9	409	1636	2	C+, Ra	intrusives, dykes	75	1982
U.K. Ardnamurchan igneous complex	59.5	3	77	175	3.3	4.2	56.7	−6.2	62	484	3	M	intrusives	146	1984
Scotland, Mull lavas	62	2	72.2	168.3	3	4.1	56.4	−6.1	78	492	2	M	intrusives, basalts	1979	1977
Aix-en-Provence Sediments, France[b]	71.5	23	73	156	10	10	43.5	5.5	10	96	3	F+, Rc, M	sediments, sandstones, limestones	6218	1989
Northern Ireland, Antrim basalts	71.5	15	70.9	125.8	12.1	13.6	55.1	−6.4	19	79	3	M	extrusives, basalts	2493	1972
Germany, Limestones, Munster Basin	92.5	9	75.8	181.1	3.8	3.8	52	8	9	191	3	Fo, M	sediments, limestones	758	1979
Combined sills and dikes, Spitsbergen	108	7.5	61.8	222.9	6.8	8.2	77.5	17	13	150	4	Rc, M	intrusives	1493	1985
France, Berriasian limestones	142	3	74.1	183.1	3.1	4.2	44.4	4.2	1	163	4	R-, M	limestone, marls	617	1985
Norway, Hinlopenstretet Dolerites	144	5	66	200	7	8	79	20	9	157	4	M	intrusives, dolerites	6220	1989
Switzerland and France, Blue limestones	155	2.5	77.2	149	4.6	6.5	47.3	7.2	24	204	3	F+, Ro, M	sediments, limestones	427	1984
France, Terres Noires	158	3	77.6	129.7	7.1	10.1	44.5	4.3	5	40	3	F+	sediments	8204	1992
Switzerland, France, Jura Mountains Oolites	159	2	76.5	142.5	4.8	6.7	46.5	6	16	298	4	F+, Ro, M	sediments, ferriferous oolites	6501	1991
Germany, limestones	155	3	72.7	125.7	4.7	6.3	49	11	12	252	2	Ro, M	sediments, limestones	2289	1977
Poland, Oxfordian sediments	155	2	70.1	147	4.2	5.7	52.9	18	6	61	4	M	sediments, limestones	3119	1988
Poland, limestones, Krakow-Czestochowa Upland	158	7	72.3	150.4	7.7	10.6	50.3	19.5	8	55	4	Ro, M	sediments, limestones	1802	1987
Alsace, France, Jurassic sediments	168	4	63.1	120.1	6.1	8.7	48.7	7.5	7	47	4	F+, Ro, M	sediments, limestones	792	1988
Sweden, Scanian basalts	181	13	69	102	10	11	55.5	14	21	170	4	Rc, M	extrusives, basalts	7078	1993
France, Thouars and Airvault Toarcian stratotypes	183	9	70.1	102.6	5.1	5.1	48	−0.2	14	114	2	Rb	sediments	3225	1987
Yorkshire, U.K., Liassic sediments	192	6	76.9	134.7	2.5	2.5	54.6	−0.8	29	185	3	M	sediments	701	1982
Bretagne, France, Kerforne dikes	198	20	61.3	78.8	10.2	10.2	48.3	−4.5	7	76	4	M	intrusives, dolerites	7128	1993
Paris Basin sediments[b]	202	13	51.3	105	2.8	4.2	49.7	4	16	496	4	Rb, M	sediments, limestones	7820	1996

[a] See Table 1a footnote for explanation.
[b] Declinations are suspect, due to possible local tectonic rotations, and inclinations only are used (see text).

Table 1g. Selected Paleomagnetic Data for North America Used in This Study Extracted From the GPMD V3.3 Database[a]

Rock Name	Age	Dage	Plat	Plong	*Dp*	*Dm*	Slat	Slong	*B*	*N*	Dc	Tests	Rock Type	RNO	Year
Alberta, Canada and Montana, Tills and Paleosols	1	2	80.4	119.5	8.2	10.6	48.8	−113.5	22	250	4	Rc	sediments, tills, paleosols	7663	1995
Alberta, Canada and Montana, Kennedy Drift	1	2	80.4	119.5	8.2	10.6	48.8	−113.5	22	237	3	Rc	sediments, tills, paleosols	7774	1995
Wyoming and Montana, Clinker deposits	1	2	81	158	6	7.8	46	−105	17	150	3	F+, Ro, M	sediments, baked	1227	1984
Northwest Territories, Canada Katherine Creek sediment[b]	1.5	3	77.8	123.7	7.9	8.8	65	−127.6	8	100	4	Ro	sediments, tills	8031	1996
SW Wyoming, Leucite Hills Volcanics[b]	1.5	1	83.2	117.8	6.1	8.5	41.6	−109	39	232	2	Rc	intrusives	1265	1980
Colorado, Lake City Caldera[b]	23	2	76.2	210	11.2	13.6	38	−107.3	17	128	3	C+, Rc, Fo, M	extrusives, intrusives	356	1986
San Luis Basin, Colorado, Conejos and Hinsdale[b]	26	6	79.7	162.6	6.9	9.7	37.2	−105.6	23	168	4	Rc	extrusives, basalts, andesites, dacites	8164	1997
Colorado, Volcanics, San Juan Mountains[b]	30.5	9	85.2	304.3	8	10.7	37.5	−106.5	18	164	2	Rc	extrusives, intrusives	2556	1974
Labrador, Canada, Mistastin Lake Impact Structure	38	8	85.5	117.7	3.4	4	55.9	−63.4	10	73	3	N	metamorphics, impact melt rocks	3235	1969
Wyoming, East Fork, Washakia Basin sediments[b]	44	12	83.9	144.2	8.8	11.7	43	−109.5	10	85	3	Rc, Fo	sediments	1138	1986
Wyoming, Rattlesnake Hills Volcanics[b]	46	6	82.6	151.9	12.3	12.3	42.8	−107.3	9	64	2	N	extrusives	2209	1977
Wyoming, Absaroka basalts[b]	46.5	5	83.5	177.4	10.1	10.1	44.5	−110	19	91	2	Rc, M	extrusives	2014	1977
Virginia, Monterey Intrusions	47	4	87.6	45.9	12	12	38.4	−79.6	6	36	3	Rc, M	intrusives, felsite	2471	1974
Montana, Robinson Anticline Intrusive Complex	50.5	5	77.1	145.8	4.7	6.1	46.2	−111.5	16	93	3	Rc, M	intrusives, syenite, trachyte sills	458	1988
Montana, Highwood Mountains intrusions	51	4	81.2	167.3	7.1	7.1	47.4	−110.6	29	220	2	N	intrusives	1262	1980
Wasatch and Green River Formations[b]	51	4	77.8	128.4	4.8	6.9	41.6	−110.4	25	129	4	Rb	sediments, redbeds, shales, limestones	8194	1997
Montana, Bearpaw Mountains intrusions	52	4	80.5	198.4	5.8	5.8	48.2	−109.7	18	160	2	Ro	intrusives	1261	1980
Montana, Paleocene igneous rocks	63	8	81.8	181.4	5.4	5.4	47.6	−108.9	36	311	3	Rc	intrusives	293	1983
Alberta, Canada, Edmonton Group	63.5	1	72	183	10.3	11.6	51.9	−112.9	20	60	3	N	sediments	1729	1985
Montana, Alkalic intrusions	64	6	80.5	185.1	5.6	5.6	47.5	−109	33	284	2	Ro	intrusives	1264	1980
Montana, Boulder Batholith	75	10	73	249	12	13	46	−112.5	27	314	2	Ro, M	intrusives	2835	1973
Montana, Adel Mountains Volcanics	76	10	83.4	200.9	6.5	7.7	47.5	−111.9	26	193	4	F+, G+, M	extrusives, intrusives	6165	1991
Montana, Maudlow Formation	79.5	11	69.8	207.8	9.8	9.8	46.1	−111.1	11	55	4	F+, Rc	sediments, volcaniclastic	6223	1989
Montana, Elkhorn Mountains Volcanics	80	6	80.3	189.5	9.6	9.6	46.1	−112	15	112	4	F+, Rc	extrusives, andesites, sediments, volcanic	6191	1991
Arkansas Alkalic Intrusives	94	12	74.1	192.5	5.7	5.7	34.3	−92.5	20	147	4	M	intrusives	401	1988
New England Intrusions	102	3	76.6	167.5	5.3	5.3	43.6	−71.6	16	106	4	M	intrusives, syenite	8096	1996
New England Intrusions	112	2	74.5	195.2	3.8	3.8	43.5	−71	27	157	4	M	intrusives, syenite, rhyolite, gabbro	8095	1996
Quebec, Canada, Monteregian Hills intrusives	120	10	69.9	188.7	3.7	5	45.5	−73	16	74	2	Rc	intrusives	3282	1968
Quebec, Canada, Monteregian intrusives	120	10	71.3	189.5	2.7	3.6	45.3	−72.8	32	147	2	Ro	intrusives	3178	1969
Quebec, Canada, Monteregian intrusives	120	10	72.4	191	2.8	3.7	45.3	−73.2	70	760	3	Ra	intrusives	1610	1979
Notre Dame Bay, Newfoundland, Canada, dikes	122	20	73.9	201	5.3	6.8	49.5	−55.1	15	86	3	N	intrusives, lamprophyre	5942	1981
Southern Maine intrusions	123	5	72.2	198.9	3.3	3.3	43.3	−70.7	41	236	4	R+, M	intrusives, gabbro, granodiorite, diorite	7837	1996
Quebec, Canada, Mount Megantic intrusions	130	20	75.2	181.4	4.2	5.9	42.4	−71.2	44	101	3	Rb, Co	intrusives, gabbro, granite, syenite	1724	1985
Notre Dame Bay, Newfoundland, Canada, dikes	135	30	67	212	4.3	5.6	49.5	−55.5	10	68	3	N	intrusives, lamprophyre	1611	1979
New York, Ithaca kimberlites	142	8	58	203.1	3.8	3.8	42.5	−76.5	7	48	4	Rb, C+, M	intrusives, kimberlite	6871	1993
Louisiana, Winfield Salt Dome Cap Rock	152	11	76.2	120.5	2.8	4.9	31.9	−92.6		100	4	Ro, M	sediments, anhydrite	7674	1993
Wyoming, Twin Creek Formation[b]	168	21	83	286	12	15	43.2	−110.5	8	60	4	F*+	sediments, limestones	6010	1990
Vermont, New Hampshire, White Mountains Plutons	169	16	88.4	82.1	6.1	6.1	44	−71.5	10	50	4	N	intrusives, granite, syenite, diorite	6018	1990
North Carolina, northwest dikes	180	30	52.6	60.7	4.9	9.8	36	−79.8	11	77	3	N	intrusives	1517	1987
North Carolina, north-south dikes	180	30	69.6	47.1	5.5	9.2	36	−79.8	15	100	3	Ro	intrusives	1518	1987
Vermont, New Hampshire, White Mountain Volcanics	180	20	85.5	124.5	4.5	6	44	−71	12	130	2	Rb	extrusives	3434	1966
New Brunswick, Canada, Caraquet dike	191	5	74.1	114	7.6	11.4	46.8	−66	8	36	3	M	intrusives, dolerite	1661	1981

Table 1g. (continued)

Rock Name	Age	Dage	Plat	Plong	*Dp*	*Dm*	Slat	Slong	*B*	*N*	Dc	Tests	Rock Type	RNO	Year
North Carolina, northwest dikes	180	30	52.6	60.7	4.9	9.8	36	−79.8	11	77	3	N	intrusives	1517	1987
North Carolina, north-south dikes	180	30	69.6	47.1	5.5	9.2	36	−79.8	15	100	3	Ro	intrusives	1518	1987
Vermont, New Hampshire, White Mountain Volcanics	180	20	85.5	124.5	4.5	6	44	−71	12	130	2	Rb	extrusives	3434	1966
New Brunswick, Canada, Caraquet dike	191	5	74.1	114	7.6	11.4	46.8	−66	8	36	3	M	intrusives, dolerite	1661	1981
Nova Scotia, Canada, North Mountain Basalt	191	10	73	104	4.5	6.5	44.9	−65.4	25	40	2	G+, M	extrusives, basalts	3280	1968
South Carolina Piedmont, Diabase dikes	194	8	66.1	96.1	4.9	9.3	34.3	−81.5	20	80	3	N	intrusives	1477	1982
South Carolina Piedmont, Diabase dikes	194	8	66.1	96.1	4.9	9.3	34.3	−81.5	20	80	3	N	intrusives	1477	1982
Combined Pennsylvania diabase	195	10	62	104.5	1.5	1.5	40.2	−76.3	78	375	2	N	intrusives, diabase	2461	1972
Connecticut Valley Volcanics	198	15	65.5	87.5	7.2	12.6	41.5	−72.7	7	313	2	N	extrusives, intrusives	3546	1968
Newark Group	200	20	63	108	3	4	40.5	−75	29	78	3	N	sediments, redbeds, extrusives, intrusives	3610	1961
Newark Supergroup Volcanics	201	14	68	88.6	3.9	3.9	42	−73	7	49	4	M	extrusives, intrusives, diabase	5963	1989
Pennsylvania, Culpeper Basin intrusives and baked sediments	201	14	65.5	73.1	3.7	3.7	39	−77.5	16	80	4	C+	intrusives, metamorphics, baked sediments	7235	1994
New Jersey, Newark Basin Hettangian red beds	206	5	55.5	94.5	5.4	5.4	40.5	−74.3	11	53	4	N	sediments, red beds	6020	1990
New Jersey, Passaic Formation, Preakness Basalt	208	3	62.2	115.1	10.5	10.5	40.5	−75	6	89	3	C+	sediments, red beds, extrusives, basalts	1232	1986

[a] See Table 1a footnote for explanation.
[b] See Table 1f.

Gordon, 1984]. Despite the huge number of cores which have been drilled in recent decades in the various steps of international drilling projects, only a few reliable data can be used for the determination of paleolatitudes. *Peirce* [1976, 1978] provided early compilations of these data, and selected the most reliable studies. One of the main problems encountered in oceanic cores is the absence of orientation: declination is not available, unless one uses the present Earth's field to reorient the core. Inclination alone allows only the determination of small circles of equal paleocolatitude on which the pole must lie. Another problem is the underestimation of inclination due to arithmetic averaging (but see *Enkin and Watson* [1996]). In order to overcome this problem, *Peirce* [1976] used an unpublished method of Cox, which also gives an estimate of the standard error (S_M). We have selected those data corresponding to values of S_M less than 5°. A minimum amount of 36 samples in a study was used, as was the case for terrestrial paleomagnetic poles.

[18] In addition, as regards data postdating the *Peirce* [1976, 1978] compilations, we have used the paleomagnetic studies of oceanic cores drilled during campaigns of the Ocean Drilling (ODP) and Deep Sea Drilling (DSDP) Projects in the Indian (Wharton Basin and Ninety-East Ridge) and South Atlantic (South American plate) Oceans. We used the Leg 73 paleolatitudes published by *Tauxe et al.* [1983], and the Leg 115 data of *Schneider and Kent* [1990a] and *Vandamme and Courtillot* [1990]. The latter studies give paleolatitudes for both the Indian and African plates. All these results are listed in Table 2b. The distribution of these data, altogether representing 19 determinations from 0 to 120 Ma, is also plotted in Figure 1a.

2.3. Combining Data Types

[19] The space and time distributions of selected paleomagnetic data are shown in map (Figures 1a and 1b) and histogram (Figures 1c–1e) form. A total number of 242 independent data have finally been retained. This final data set comprises 221 ''classical'' poles, two poles determined using marine magnetic anomaly skewness data and 19 ''inclination only'' data from oceanic cores. The total number of data is thus increased by more than 2 with respect to the BC91 database, which comprised only 111 poles. The map (Figure 1b) shows all poles (as dots) and the corresponding sites (as stars) in (South) African coordinates, with sites restored to their relative positions at the appropriate time. We see that geographical coverage is quite reasonable; it is much improved over BC91. The histogram (Figure 1c) shows that a large number of data (more than 30) is available for the 0–30 and 50–80 Ma time windows. By contrast, the 140–150 Ma time window contains only eight studies. The mean number of data in each 10 Myr time window is on the order of 15. As a matter of comparison, the corresponding mean for the recent *Prévot et al.* [2000] study is on the order of 4, and there are less than 5 data in twelve 10 Myr time windows.

3. Kinematic Models

[20] Despite the significant improvement in the paleomagnetic database, the number of data is still rather low if one wants to construct the APWP of a single plate based on its

Table 2a. Pole Positions Deduced From Skewness of Marine Anomalies 24 and 25 in the Indian Ocean[a]

Mean Age	Anomaly	λ(°N)	ϕ(°E)	ND	95%CI	K
57.2	25	76.8	224.7	17	6.9	30.7
61.5	26	76.4	200.6	14	6.2	48.2

[a] Definitions: λ(°N), pole latitude; ϕ(°E) pole longitude; ND, number of determinations; 95%CI, confidence interval; *K*, precision parameter.

own paleomagnetic poles only. As in BC91, we therefore take advantage of the fact that the APWPs from individual plates cannot be independent one from the other and should be related through plate kinematic models. And indeed, accurate up-to-date models are available for the Indian, North Atlantic, central Atlantic, and South Atlantic Oceans, allowing one to relate the seven selected plates over the entire period of interest here with reasonable confidence. A possible motion between Eurasia and North America [*Van der Voo*, 1993] may constitute a source of error during Jurassic times. These models can be used to transfer all paleomagnetic data to a common, single reference frame, arbitrarily taken here to be the southern part of the African plate.

[21] *Müller et al.* [1993] have published a new set of data, in which plate motions with respect to hot spots are computed based on combined Atlantic and Indian Ocean hot spot tracks between the Present and 130 Ma. The initial relative plate motion parameters are those quoted in the database of *Royer et al.* [1992], and are computed at any given age for the same anomaly. We have taken advantage of these compilations, both because of their unifying features, and because one of the aims of this paper is indeed to compute relative motions between the paleomagnetic and hot spot reference frames. *Müller et al.* [1993] extensively discuss the implications of their plate motion models. Two important features of their reconstructions are the internal deformation of the African and South American plates during breakup phases in the Cretaceous, and a new model of the final breakup of Gondwana, in which India rifted away from Antarctica at the same time it rifted away from Australia (i.e., between chrons M10 and M11).

[22] On the basis of the *Royer et al.* [1992] and *Müller et al.* [1993] kinematics, we have recomputed the relative motions at the time of each anomaly between 0 and 130 Ma, by simply subtracting the absolute motion of (South) Africa with respect to hot spots from the motion of other plates (Table 3). The finite poles of rotation which are not given by *Müller et al.* [1993] are those of *Müller and Roest* [1992] for the motion between Europe and North America, and those of *Srivastava and Tapscott* [1986] for Greenland and North America. They were combined with the North America versus South Africa motion to obtain total motion with respect to South Africa. The Arabia to Africa rotation poles are those of *Le Pichon and Gaulier* [1988]. For periods earlier than 130 Ma, the South America to South Africa kinematic parameters are those of *Nürnberg and Müller* [1991], the Australia to East-Antarctica to South Africa rotation poles are those of *Royer and Sandwell* [1989], using respectively a recomputed fit and a fit after *Lawver and Scotese* [1987]. Prior to 130 Ma, the Madagascar to South Africa motion uses the parameters from the Global Isochron Chart of *Royer et al.* [1992], with a final fit from *Lawver and Scotese* [1987].

[23] For each plate, paleomagnetic or skewness poles and small circles based on DSDP/ODP inclination data were transferred onto (South) Africa. For this, we interpolated a Eulerian pole of rotation between the two published finite rotation poles with ages bracketing the estimated age respectively of the pole and drill hole or crustal block corresponding to the individual datum. Errors incurred in such reconstructions are unlikely to exceed 2° (see *Molnar and Stock* [1987], discussion by *Besse and Courtillot* [1988, 1991], and *Acton and Gordon* [1994]). We must be cautious in case the timescales used by different authors are not identical and therefore require some discussion. *McElhinny and Lock* [1995] used the *Harland et al.* [1989] timescale, whereas *Müller et al.* [1993] used that of *Kent and Gradstein* [1986]. We have compared the differences in the ages of each particular chron or anomaly, and of geological stage boundaries, when the two different timescales are used. Between 120 Ma and the Present, the corresponding mean age differences are generally less than 1 Myr, with a maximum of 1.4 Myr between 55 and 170 Ma. Between 120 and 130 Ma (i.e., from the Valanginian to the early Aptian), the difference reaches 4 to 7.5 Ma, but this is a time

Table 2b. Selected Data From ODP and DSDP Legs[a]

Mean Age	Sλ (°N)	Sϕ (°E)	Colatitude	NC	95%CI	Site	Plate	Rock Type	Author
3.3	−26.1	−5.1	121.7	83	4.2	519	AFR	s	*Tauxe et al.* [1983]
15	20.1	61.5	82	49	4.1	222	IND	s	*Pierce* [1976]
18	−26.1	−10.3	123.7	98	3.1	521	AFR	s	*Tauxe et al.* [1983]
26	−26.1	−5.1	121.2	55	3.1	522	AFR	s	*Tauxe et al.* [1983]
27.5	−28	−36.3	104.7	42	4.4	17	AMS	s	*Pierce* [1976]
28	−26.1	−5.1	122.9	100	1.5	522	AFR	s	*Tauxe et al.* [1983]
32.5	−28.5	−2.2	123.8	65	4.4	523	AFR	s	*Tauxe et al.* [1983]
40.3	−28.5	−2.2	132.3	82	2.7	523	AFR	s	*Tauxe et al.* [1983]
45.5	−28.5	−2.2	133.5	102	3.8	523	AFR	s	*Tauxe et al.* [1983]
47	−4.2	73.4	102.3	52	1.8	713	IND	v	*Vandamme and Courtillot* [1990]
54.7	−24.9	87.4	141.9	49	3	253	IND	s	*Pierce* [1976]
57.5	−19.2	99.3	119.7	38	4.8	212	AUS	s	*Pierce* [1976]
63.9	−29.5	3.5	135.9	257	2.6	524	AFR	s	*Tauxe et al.* [1983]
66	−7.5	59	115.2	56	4.2	707	AFR	v	*Vandamme and Courtillot* [1990]
104.5	−16.1	116.3	116.7	61	3.9	260	AUS	s	*Pierce* [1976]
114.5	−23.3	111	135.9	44	4.7	263	AUS	s	*Pierce* [1976]
114.5	−23.3	111	132	106	2.9	263	AUS	s	*Pierce* [1976]

[a] Sλ(°N), site latitude; Sϕ(°E) site longitude; colatitude, paleomagnetic colatitude; NC, number of samples; 95%CI, confidence interval; site, number, plate to which datum belongs; rock type, s, sediment ; v, volcanics; author, reference.

Table 3. Finite Rotation Poles for Gondwana[a]

	NW Africa onto South Africa					Arabia onto South Africa				
An	Age, Ma	λ(°N)	ϕ(°E)	ω, deg	Source	Age, Ma	λ(°N)	ϕ(°E)	ω, deg	Source
A34	84.0	0.0	0.0	0.0		4.7	32.75	22.64	−1.89	(2)
	100.0	−17.3	−172.8	5	(1)	13	32.15	22.59	−5.36	(2)
	110.0	−15.7	−174.0	.9	(1)	30	32.11	22.57	−7.36	(2)
M0	118.7	−18.1	−173.6	1.1	(1)					
M10	130.0	29.8	15.2	1.6	(1)					

		East Antarctica to South Africa				India to South Africa				Australia to South Africa			
An	Age, Ma	λ(°N)	ϕ(°E)	ω, deg	Source	λ(°N)	ϕ(°E)	ω, deg	Source	λ(°N)	ϕ(°E)	ω, deg	Source
5	10.4	7.9	−49.5	1.5	(1)	−23.7	−146.7	4.6	(1)	−11.9	−130.4	6.6	(1)
6	20.5	10.8	−48.0	2.8	(1)	−29.6	−156.2	7.6	(1)	−14.5	−133.5	11.76	(1)
13	35.5	14.1	−50.7	5.5	(1)	−21.4	−139.3	15.3	(1)	−13.3	−130.6	20.16	(1)
18	42.7	15.5	−44.8	7.2	(1)	−23.6	−138.1	17.9	(1)	−15.9	−130.8	22.76	(1)
21	50.3	10.3	−42.9	8.8	(1)	−23.7	−144.1	22.1	(1)	−16.0	−127.6	23.76	(1)
25	58.6	5.3	−39.1	10.3	(1)	−23.3	−152.7	28.6	(1)	−15.9	−122.7	24.16	(1)
31	68.5	1.1	−41.6	11.8	(1)	−20.5	−160.8	42.4	(1)	−11.4	−118.2	25.66	(1)
33y	73.6	−1.9	−41.4	13.5	(1)	−22.2	−162.3	45.7	(1)	−13.5	−115.2	26.36	(1)
33o	80.2	−4.6	−39.7	16.0	(1)	−23.9	−163.2	48.8	(1)	−16.3	−110.5	27.16	(1)
34	84.0	−2.6	−38.1	17.9	(1)	−22.9	−161.2	51.0	(1)	−14.7	−106.3	27.86	(1)
	90.0	−3.9	−33.2	22.1	(1)	−22.5	−156.4	53.0	(1)	−15.7	−97.8	29.06	(1)
	100.0	−5.6	−29.0	29.3	(1)	−21.4	−149.3	56.8	(1)	−18.0	−85.0	31.86	(1)
	110.0	−6.5	−26.1	36.6	(1)	−21.4	−149.3	56.8	(1)	−20.5	−73.8	35.36	(1)
M0	118.7	−7.1	−24.4	43.1	(1)	−21.7	−148.4	57.0	(1)	−22.0	−65.7	39.26	(1)
M10	130.0	−11.9	−21.0	50.4	(1)	−22.3	−143.1	61.0	(1)	−28.2	−56.9	43.56	(1)
M16	140.0	−7.0	−26.9	50.70	(3)	−21.3	−139.0	64.7	(4)	−21.7	−63.8	46.9	(5)
M21	150.0	−4.7	−29.0	52.84	(3)	−21.6	−135.2	66.6	(4)	−19.2	−63.7	49.7	(5)
FIT	165.0	−7.8	−31.4	58.0	(5)	−26.9	−133.4	67.8	(4)	−22.6	−62.7	55.2	(5)

		Madagascar to South Africa			
An	Age, Ma	λ(°N)	ϕ(°E)	ω, deg	Source
M0	118.7	3.5	−76.3	0.9	(1)
M10	130.0	3.4	−79.2	6.9	(1)
M16	141.9	5.40	−76.20	8.32	(6)
M21	149.9	4.00	−71.40	11.32	(6)
FIT	165.0	−3.41	−81.70	19.73	(7)

[a] Recomputed following (1) *Müller et al.* [1993]; (2) *Le Pichon and Gaulier* [1988]; (3) *Royer et al.* [1988]; (4) India to South Africa motion is India to East Antarctica [*Royer and Sandwell*, 1989] plus East Antarctica to South Africa [*Royer et al.*, 1988]; (5) Australia to South Africa motion is Australia to East Antarctica [*Royer and Sandwell*, 1989] plus East Antarctica to South Africa [*Royer et al.*, 1988]; (6) *Royer et al.* [1988]; and (7) *Lawyer and Scotese* [1987].

window with no sedimentary data. From 135 Ma back to the earliest seafloor spreading anomalies at 160 Ma, the differences are between 0 and 2.8 Myr, averaging 1 Myr in absolute value. Prior to 160 Ma, only geological age assignments of formations from which paleomagnetic data are available are used and not plate kinematic parameters. For our purpose, these differences are smaller than the uncertainties in age determinations in most paleomagnetic studies, and often less than the error due to reassigning an age to an anomaly when the exact time feature used in pointing the anomaly is not accurately known. We have therefore used ages as given by the original authors, regardless of the timescale they used. However, as mentioned above in the discussion of the new paleomagnetic database, we have scaled the ages of all DSDP/ODP sites using the *Harland et al.* [1989] timescale.

4. New Synthesized APWPs

4.1. African APWP: Old and New

[24] All data and sites are shown in Figures 1a and 1b in (South) African coordinates, together with average poles (Table 4) calculated every 10 Myr with a 20 Myr window, using a method derived from *McFadden and McElhinny* [1988] in order to combine poles and small circles (this is done by iteratively finding a direction such that the Fisher average of pole directions and the points on the small circle which are closest to this direction are statistically the same).

[25] In order to give some feeling for the quality of individual means, four examples showing the poles and sites on an appropriate plate reconstruction are given for 20, 60, 90, and 200 Myr in Figure 2. Thirty-nine individual data are available for the 20 Myr reconstruction (Figure 2a), with good longitudinal and latitudinal coverage. The corresponding pole distribution is Fisherian and the 95% confidence interval is less than 3°. Data come from most major plates. The 60 Myr reconstruction (Figure 2b) involves 46 data; the distribution is approximately Fisherian with a 95% confidence interval of 3°, although several poles streak E-W, east of (65°N, 270°E). There are no data from South America. The 90 Myr reconstruction (Figure 3a) contains only 13 data with a 95% confidence interval of 2.9°, but geographical coverage is quite good, with all major landmasses except Antarctica providing compatible data. There are still 20 data available for the 200 Myr reconstruction (Figure 3b), again with most plates (except South America) in their Pangea configuration represented, a good Fisherian pole distribution and a 95% confidence interval of about 4°. Altogether, the A_{95} values range from 2 to 7°, with only a slight degradation as one goes back in time (Figure 1d). The

Table 4. Master Apparent Polar Wander Path for the Past 200 Myr Calculated for a 20 Myr Sliding Window Every 10 Myr[a]

			South Africa				South America				India				Australia			
Window	Age	*N*	λ (°N)	ϕ (°E)	A_{95}	*K*	λ (°N)	ϕ (°E)	A_{95}	*K*	λ (°N)	ϕ (°E)	A_{95}	*K*	λ (°N)	ϕ (°E)	A_{95}	*K*
0	3.1	30	86.5	171.6	2.6	105.3	86.3	172	2.6	105.1	86.1	174.8	2.6	105.2	86.1	174.8	2.6	105.2
10	8.3	54	86.0	160.8	2.0	95.8	85.4	162.5	2.0	94.4	85.0	168.1	2.0	94.2	85.0	168.1	2.0	94.2
20	18.9	38	85.4	151.9	2.7	75.9	84.0	154.8	2.7	76.2	83.3	164.2	2.7	75.6	83.3	164.2	2.7	75.6
30	29.5	23	85.1	162.2	3.8	65.6	82.8	158.1	3.8	66.2	81.5	169.2	3.8	65.4	81.5	169.2	3.8	65.4
40	40.0	24	84.3	172.4	3.3	82.1	81.3	162.4	3.3	81.9	79.5	174.4	3.2	85.5	79.1	175.1	3.2	87.5
50	52.2	31	84.7	174.7	3.4	60.1	80.9	164.4	3.4	59.4	77.9	179.3	3.4	58.2	76.3	178.0	3.4	59.7
60	59.7	45	84.7	217.6	2.8	57.4	81.1	190.5	2.9	56.1	75.9	196.8	2.9	54.7	74.4	191.3	2.8	57.2
70	67.3	34	83.8	241.6	3.2	60.3	80.3	204.3	3.2	61.0	74.2	204.8	3.2	61.2	72.9	197.9	3.2	61.7
80	77.9	14	84.7	275.8	6.0	45.1	81.4	206.1	5.9	47.2	74.7	207.4	5.9	47.0	73.1	202.2	6.0	45.7
90	90.0	13	85.0	320.8	5.3	61.7	82.2	202.1	5.2	65.2	75.5	207.4	5.1	65.9	72.9	203.8	5.1	67.2
100	97.6	12	85.5	9.7	6.8	42.0	81.7	180.1	6.7	43.0	76.6	195.8	6.7	43.1	73.0	194.4	6.7	43.0
110	113.6	17	77.7	20.2	4.1	76.7	80.0	183.6	4.2	74.8	75.1	193.8	4.2	75.3	71.3	194.5	4.2	75.0
120	119.1	20	76.4	17.3	2.3	209.6	78.2	189.4	2.4	182.9	73.1	193.9	2.4	184.3	69.3	196.0	2.4	183.7
130	126.4	14	75.3	14.0	3.2	154.5	75.8	192.9	2.8	205.5	70.6	193.0	2.8	205.6	66.8	196.5	2.8	205.8
140	136.8	7	72.4	5.8	6.5	87.4	73.8	197.6	6.0	103.2	68.3	194.2	6.0	103.4	64.6	198.4	6.0	103.4
150	151.6	10	67.0	26.6	6.8	50.8	75.0	159.9	6.6	54.3	73.6	167.7	6.6	54.5	68.7	175.2	6.6	54.4
160	162.3	15	62.9	31.6	5.0	58.5	72.5	144.0	5.0	59.7	73.7	149.7	5.0	59.7	68.4	161.3	5.0	59.7
170	173.4	21	56.9	39.3	6.0	28.8	69.7	112.5	6.7	23.6	75.5	110.1	6.7	23.6	70.9	131.8	6.7	23.6
180	178.8	18	53.2	45.7	5.4	41.3	65.5	95.9	5.6	39.7	73.0	83.4	5.6	39.7	69.9	109.2	5.6	39.7
190	189.7	23	54.5	45.0	4.2	52.9	65.3	98.4	4.2	52.9	72.6	86.8	4.2	52.9	69.3	111.8	4.2	52.9
200	196.7	19	58.2	46.9	4.3	61.6	63.2	106.0	4.3	61.6	69.8	95.6	4.3	61.6	66.1	117.7	4.3	61.6
			Antarctica				Europe				North America				Greenland			
Window	Age	*N*	λ (°N)	ϕ (°E)	A_{95}	*K*	λ (°N)	ϕ (°E)	A_{95}	*K*	λ (°N)	ϕ (°E)	A_{95}	*K*	λ (°N)	ϕ (°E)	A_{95}	*K*
0	3.1	30	86.5	171.6	2.6	105.3	86.3	172	2.6	105.1	86.1	174.8	2.6	105.2	86.1	174.8	2.6	105.2
10	8.3	54	86.0	160.8	2.0	95.8	85.4	162.5	2.0	94.4	85.0	168.1	2.0	94.2	85.0	168.1	2.0	94.2
20	18.9	38	85.4	151.9	2.7	75.9	84.0	154.8	2.7	76.2	83.3	164.2	2.7	75.6	83.3	164.2	2.7	75.6
30	29.5	23	85.1	162.2	3.8	65.6	82.8	158.1	3.8	66.2	81.5	169.2	3.8	65.4	81.5	169.2	3.8	65.4
40	40.0	24	84.3	172.4	3.3	82.1	81.3	162.4	3.3	81.9	79.5	174.4	3.2	85.5	79.1	175.1	3.2	87.5
50	52.2	31	84.7	174.7	3.4	60.1	80.9	164.4	3.4	59.4	77.9	179.3	3.4	58.2	76.3	178.0	3.4	59.7
60	59.7	45	84.7	217.6	2.8	57.4	81.1	190.5	2.9	56.1	75.9	196.8	2.9	54.7	74.4	191.3	2.8	57.2
70	67.3	34	83.8	241.6	3.2	60.3	80.3	204.3	3.2	61.0	74.2	204.8	3.2	61.2	72.9	197.9	3.2	61.7
80	77.9	14	84.7	275.8	6.0	45.1	81.4	206.1	5.9	47.2	74.7	207.4	5.9	47.0	73.1	202.2	6.0	45.7
90	90.0	13	85.0	320.8	5.3	61.7	82.2	202.1	5.2	65.2	75.5	207.4	5.1	65.9	72.9	203.8	5.1	67.2
100	97.6	12	85.5	9.7	6.8	42.0	81.7	180.1	6.7	43.0	76.6	195.8	6.7	43.1	73.0	194.4	6.7	43.0
110	113.6	17	77.7	20.2	4.1	76.7	80.0	183.6	4.2	74.8	75.1	193.8	4.2	75.3	71.3	194.5	4.2	75.0
120	119.1	20	76.4	17.3	2.3	209.6	78.2	189.4	2.4	182.9	73.1	193.9	2.4	184.3	69.3	196.0	2.4	183.7
130	126.4	14	75.3	14.0	3.2	154.5	75.8	192.9	2.8	205.5	70.6	193.0	2.8	205.6	66.8	196.5	2.8	205.8
140	136.8	7	72.4	5.8	6.5	87.4	73.8	197.6	6.0	103.2	68.3	194.2	6.0	103.4	64.6	198.4	6.0	103.4
150	151.6	10	67.0	26.6	6.8	50.8	75.0	159.9	6.6	54.3	73.6	167.7	6.6	54.5	68.7	175.2	6.6	54.4
160	162.3	15	62.9	31.6	5.0	58.5	72.5	144.0	5.0	59.7	73.7	149.7	5.0	59.7	68.4	161.3	5.0	59.7
170	173.4	21	56.9	39.3	6.0	28.8	69.7	112.5	6.7	23.6	75.5	110.1	6.7	23.6	70.9	131.8	6.7	23.6
180	178.8	18	53.2	45.7	5.4	41.3	65.5	95.9	5.6	39.7	73.0	83.4	5.6	39.7	69.9	109.2	5.6	39.7
190	189.7	23	54.5	45.0	4.2	52.9	65.3	98.4	4.2	52.9	72.6	86.8	4.2	52.9	69.3	111.8	4.2	52.9
200	196.7	19	58.2	46.9	4.3	61.6	63.2	106.0	4.3	61.6	69.8	95.6	4.3	61.6	66.1	117.7	4.3	61.6

[a] Window, age of the center of window; age, mean age computed from the data; *N*, number of studies; λ, ϕ, latitude and longitude of mean VGP; A_{95} uncertainty at the 95% confidence level; *K*, Fisher's precision parameter.

overall mean A_{95} is 2.9 ± 0.8° (1σ) for the new synthesized APWP, significantly less than the value of 4.1 ± 1.2° found by BC91; the decrease (4.1/2.9 = 1.4) is not much less than the maximum value ($\sqrt{2.2}$ = 1.5) expected from increasing the number of data.

[26] There are enough data that a significant synthetic APWP can be calculated with a time resolution increased by a factor of 2, i.e., one average every 5 Myr with a 10 Myr time window (Table 5). This results in a mean A_{95} of 4.2 ± 1.9°, i.e., similar to BC91 with a twofold increase in time resolution.

[27] We have plotted in Figure 4 the angular test parameter $\gamma_c - \gamma_o$ [from *McFadden and McElhinny*, 1990], determined for pairs of poles consisting of the calculated mean pole from each plate versus the corresponding overall mean (synthesized) pole for the same 20 Myr time window, as a function of age. Pole pairs are not significantly different at the 95% probability level when the test parameter is positive. Four apparently discrepant poles deserve some comment. Two poles appear to be significantly different from the coeval synthesized pole: those for NAM in the 0–10 Myr window and EUR at 70 Ma (60–80 Myr window). For the NAM pole, there are only 6 data and the discrepancy could for instance be due to a slightly larger quadrupole term, on the order of 10% of the axial dipole (for the last few million years, ranges of estimates are between 3 and 8% [*Schneider and Kent*, 1988; *McElhinny et al.*, 1996; *Johnson and Constable*, 1997; *Carlut and Courtillot*, 1998]). The pole from EUR is based on a combination of only three studies, all being to some extent questionable. One study comes from the Aix-en-Provence series (south of France), in which rotations have subsequently been revealed. The two other studies are from the Antrim and Mull lavas of the British Tertiary Igneous Province. Their

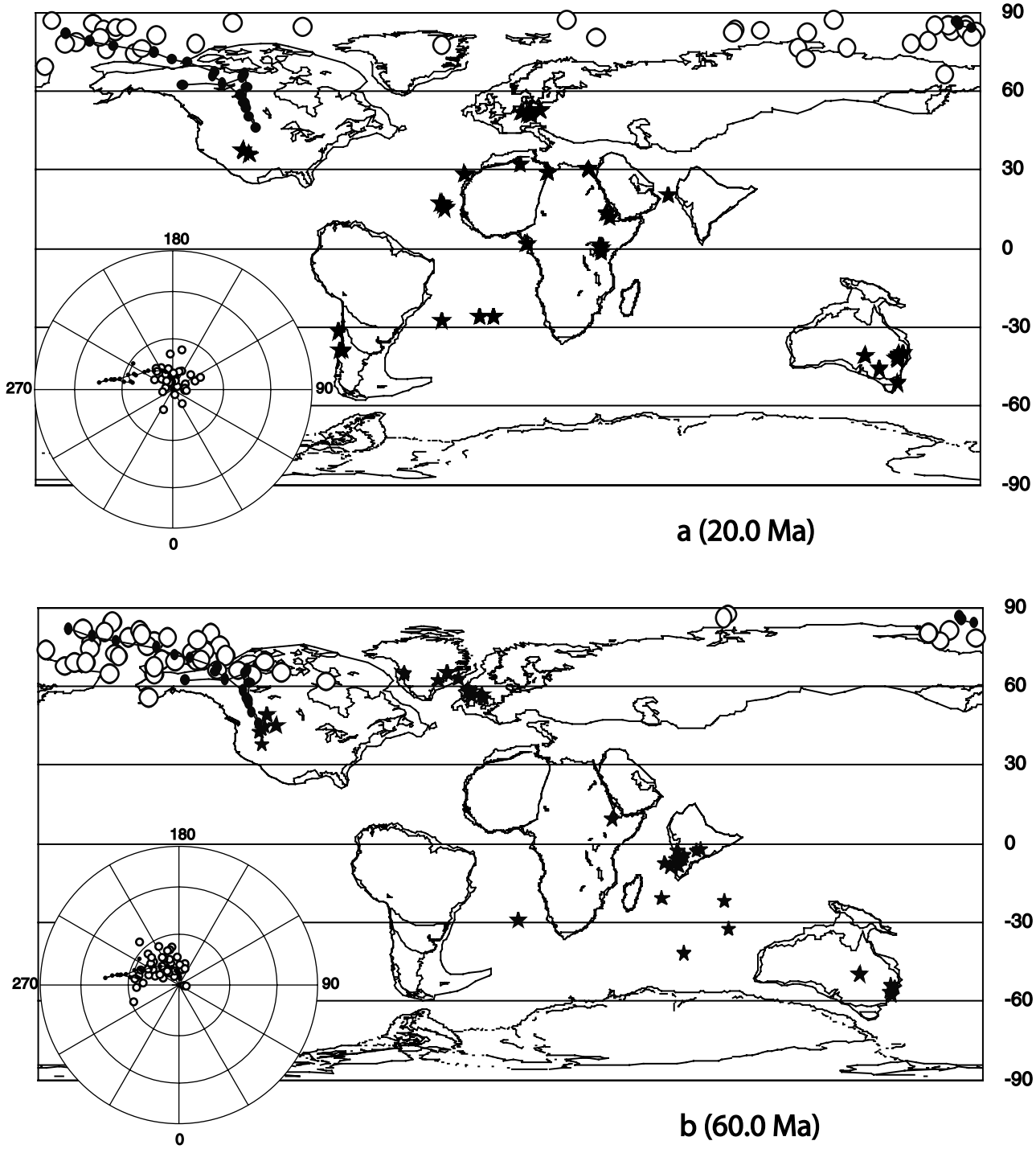

Figure 2. Plate reconstructions at (a) 20 and (b) 60 Ma in rectilinear projection, together with transferred poles in equal-area projection (the South African plate is kept fixed in longitude). The transferred poles and site locations are also shown as open circles and solid stars, respectively, in the projections. Insets: polar view of the synthetic African APWP (small linked dots) with all data for the appropriate time window (larger open circles).

ages in the database (around 70 Ma) are now known to be too old by some 10 Myr when compared with more recent estimates based on a combination of new radiometric ages and the magnetic polarity timescale [*Saunders et al.*, 1997]. Indeed, a large part of these lavas erupted during reversed chron C26r dated at 59 ± 1 Myr. Such an error in the assigned age may easily account for the observed discrepancy. For two poles, there is a problem of rounding the age at a time of significant change. Such is the case for the 50–60 Ma Australian pole and for the 160–170 Ma Greenland pole. The effect of the slight differences in ages of observed versus predicted poles illustrates difficulties linked to the

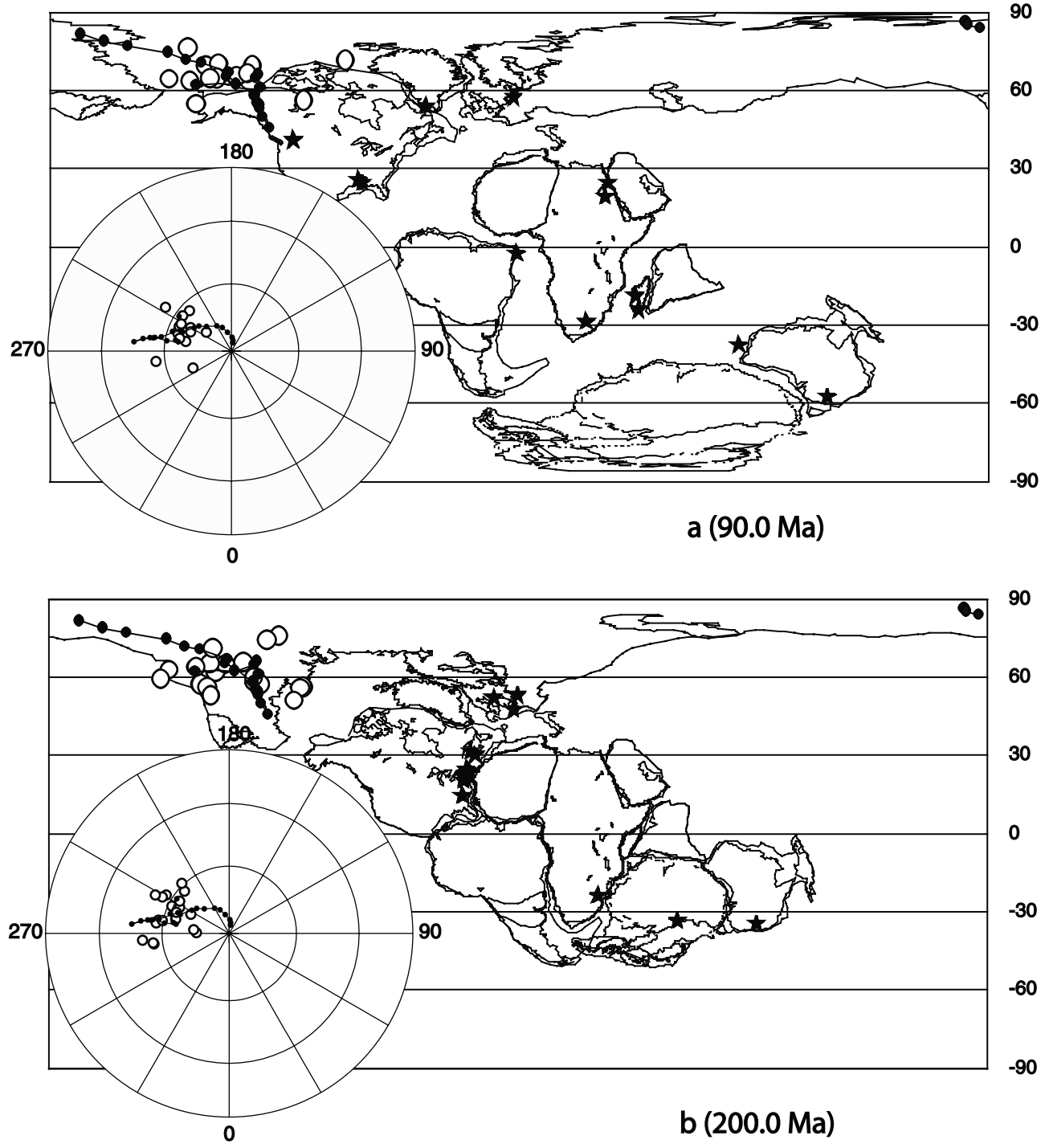

Figure 3. Plate reconstructions at (a) 90 and (b) 200 Ma. Same legend as Figure 2.

sparseness of the database and can lead to misleading tectonic or field-geometry interpretations. For instance the calculated 54.4 ± 5.2 Myr mean pole from AUS data only can be compared either with either the 55 or 59 Myr overall mean (synthesized) pole, in one case with a discrepancy, in the other with none. A similar case is also shown for GRE at 160–170 Ma. Note again (as in Figure 1d) that there is no sign of degradation with age.

[28] In Figure 5, we compare three synthesized APWPs in (south) African coordinates: triangles are for the original BC91 curve, dots for the new BC01 curve, and stars for an APWP computed with the BC91 database but with the updated kinematics used in the present paper (BC91'). The 0–140 Ma and 120–200 Ma segments are shown separately in Figure 5 to avoid too much overlap and lack of legibility. We first see that improvement in the kinematic models results in insignificant changes from the Present back to 160 Ma. On the other hand, the 170 (actually 175) and 180 (actually 178–179) Ma poles are significantly displaced. This is essentially due to a different Gondwana fit (see section 4, APWP for Africa).

[29] Now, comparing BC91 and BC01, we see that the increased database has resulted in a systematic ~2° shift of

Table 5. Synthetic Apparent Polar Wander Path for the Past 200 Myr Calculated for a 10 Myr Sliding Window Every 5 Myr[a]

			South Africa				South America				India				Australia			
Window	Age	*N*	λ (°N)	ϕ (°E)	A_{95}	*K*	λ (°N)	ϕ(°E)	A_{95}	*K*	λ (°N)	ϕ (°E)	A_{95}	*K*	λ (°N)	ϕ (°E)	A_{95}	*K*
0	2.1	25	86.6	182.2	3.0	96.2	86.8	176.3	3.0	96.0	87.0	197.1	3.0	95.7	87.5	204.0	3.0	95.1
5	3.1	30	86.2	176.9	2.6	105.5	86.5	168.0	2.6	104.8	86.8	197.1	2.6	106.2	87.5	207.6	2.6	105.1
10	11.9	21	85.0	170.7	3.1	107.4	85.5	139.9	3.1	107.3	85.8	231.1	3.1	104.0	85.9	277.2	3.2	100.9
15	14.8	24	84.2	170.9	3.2	85.1	84.8	136.7	3.2	84.2	84.9	231.2	3.2	86.8	84.9	279.3	3.2	89.0
20	19.6	16	81.7	165.7	4.5	69.3	82.1	131.8	4.6	66.4	83.4	221.9	4.5	70.0	84.1	273.0	4.5	69.3
25	26.0	14	83.4	184.5	5.4	55.8	84.4	126.1	5.3	59.2	81.3	264.7	5.7	50.8	78.6	294.7	5.7	50.8
30	30.2	13	79.0	207.7	5.4	63.3	83.5	163.8	5.3	64.7	74.9	263.6	5.0	72.3	73.0	282.8	5.0	72.4
35	33.7	12	78.9	201.7	4.5	96.1	82.9	152.1	4.7	89.4	75.1	266.3	4.5	96.6	72.9	285.3	4.5	96.5
40	39.0	8	77.3	191.6	7.2	63.3	80.0	139.5	7.3	62.0	74.9	264.4	7.2	63.7	73.2	283.7	7.1	64.7
45	46.4	12	79.1	200.6	5.2	73.0	82.0	126.5	5.3	72.6	70.6	277.8	5.5	67.1	70.2	294.6	5.4	69.1
50	49.9	17	78.7	204.1	4.2	74.5	82.2	127.7	4.2	75.5	67.7	278.5	4.5	66.1	69.5	295.7	4.1	76.4
55	55.0	22	76.7	214.7	4.2	56.1	82.7	145.3	4.1	57.5	60.7	277.7	4.8	43.6	67.2	294.2	4.1	58.0
60	60.7	24	73.9	224.0	4.3	48.7	82.4	168.5	4.3	48.9	50.8	277.5	4.6	42.5	64.3	292.7	4.3	48.8
65	64.0	24	71.6	234.2	3.6	67.8	82.0	193.7	3.6	68.3	42.4	279.4	4.0	56.1	60.6	293.1	3.6	67.9
70	68.3	15	71.1	237.4	4.7	67.2	82.3	199.0	4.8	65.0	36.8	281.0	4.5	74.5	59.5	295.4	4.8	65.8
75	75.4	10	72.5	232.4	7.4	44.9	83.6	170.6	7.2	46.4	33.6	282.1	7.7	41.2	62.1	300.6	7.3	45.4
80	79.1	9	68.3	251.9	7.0	56.1	82.3	228.4	6.9	57.5	25.7	287.5	7.1	54.2	54.8	303.5	6.9	58.1
85	83.4	5	66.9	253.1	9.8	61.7	82.5	229.5	10.2	57.7	22.6	289.1	9.4	67.2	54.4	305.4	10.0	59.4
90	91.4	8	66.7	242.7	3.4	259.8	84.8	175.8	3.6	232.6	21.9	289.2	3.9	200.0	59.9	309.4	3.9	203.5
95	94.1	8	66.5	246.0	6.6	72.2	86.2	178.5	6.5	74.0	20.5	291.7	7.0	63.9	59.4	313.6	6.6	71.1
100	100.2	6	68.8	254.1	11.0	39.6	87.8	29.2	11.5	35.9	19.9	298.0	10.9	40.1	59.2	327.5	11.9	33.8
105	104.6	4	62.9	251.5	25.6	15.4	88.0	179.8	24.6	16.6	14.9	295.0	25.6	15.4	58.6	322.7	24.3	17.0
110	110.8	7	58.0	261.7	8.3	57.1	85.1	264.2	8.7	52.2	8.3	297.5	8.3	56.9	53.8	326.2	8.9	49.9
115	116.4	13	56.3	260.9	2.7	235.5	86.4	261.2	2.4	313.9	6.8	297.2	2.7	240.5	54.1	330.5	2.3	342.0
120	120.1	13	51.8	260.9	3.2	163.9	83.9	238.5	3.1	178.2	2.4	296.1	3.2	166.2	52.9	327.9	2.9	204.6
125	122.8	10	50.6	260.7	3.4	197.5	83.4	233.0	3.4	197.7	0.9	296.4	3.7	173.9	53.1	328.6	3.8	166.4
130	130.9	4	49.5	265.8	7.4	156.9	82.6	252.6	7.2	163.0	−3	301.5	8.0	132.3	50.2	335.6	8.2	127.3
135	134.3	5	49.5	264.6	5.6	189.2	83.2	246.5	5.5	192.6	−3.5	301.6	5.9	167.5	49.6	335.4	6.2	152.3
140	139.3	5	43.6	265.9	8.1	90.1	77.5	238.2	8.1	90.1	−10	300.7	7.9	93.8	44.1	328.5	8.2	88.4
145	142.0	3	40.3	263.2	11.9	108.1	74.7	227.2	11.9	108.1	−12.4	297.9	11.7	111.7	43.1	323.2	12.0	107.0
150	153.9	4	59.1	255.7	6.3	216.2	85.8	61.6	6.3	216.2	5.7	308.3	6.0	231.9	50.6	352.4	6.1	231.1
155	155.7	7	58.2	258.9	3.8	253.8	87.3	39.6	3.8	253.8	4.1	309.8	3.9	244.6	48.5	351.8	3.9	245.7
160	158.9	5	53.8	257.9	7.1	117.6	88.2	189.6	7.1	117.6	1.1	307.9	6.4	145.8	47.9	346.6	6.4	144.1
165	168.0	8	52.1	260.5	9.8	33.7	86.6	228.5	9.8	33.7	−0.7	310.7	9.8	33.7	44.8	347.3	9.8	33.7
170	170.2	13	56.5	259.1	6.8	37.8	88.9	41.9	6.8	37.8	3.4	312.4	6.8	37.8	46.2	353.3	6.8	37.8
175	176.7	13	65.7	260.8	7.2	33.8	79.7	32.2	7.2	33.8	10.6	318.3	7.2	33.8	45.5	6.6	7.2	33.8
180	178.4	12	66.8	263.9	7.6	33.4	78.4	26.6	7.6	33.4	10.9	319.9	7.6	33.4	44.2	8.0	7.6	33.4
185	182.4	9	69.5	261.4	7.6	46.5	75.9	32.6	7.6	46.5	13.6	320.6	7.6	46.5	44.9	11.9	7.6	46.5
190	191.3	13	62.9	258.9	5.5	58.4	82.5	37.0	5.5	58.4	8.8	316.0	5.5	58.4	46.4	2.6	5.5	58.4
195	194.4	14	61.7	257.9	4.9	67.9	83.7	41.6	4.9	67.9	8.0	314.9	4.9	67.9	46.9	0.8	4.9	67.9
200	198.9	8	63.9	244.6	5.7	94.9	78.8	70.6	5.7	94.9	13.7	311.7	5.7	94.9	52.6	5.8	5.7	94.9

			Antarctica				Europe				North America				Greenland			
Window	Age	*N*	λ (°N)	ϕ(°E)	A_{95}	*K*	λ (°N)	ϕ (°E)	A_{95}	*K*	λ (°N)	ϕ(°E)	A_{95}	*K*	λ (°N)	ϕ(°E)	A_{95}	*K*
0	2.1	25	86.8	178.8	3.0	96.0	86.7	178.7	3.0	96.1	86.5	180.7	3.0	96.2	86.5	180.7	3.0	96.2
5	3.1	30	86.5	171.6	2.6	105.3	86.3	172.0	2.6	105.1	86.1	174.8	2.6	105.2	86.1	174.8	2.6	105.2
10	11.9	21	85.9	151.8	3.1	107.3	85.0	155.7	3.1	107.6	84.6	164.4	3.1	107.7	84.6	164.4	3.1	107.7
15	14.8	24	85.2	151.0	3.2	85.1	84.2	154.9	3.2	84.3	83.6	163.0	3.2	84.2	83.6	163.0	3.2	84.2
20	19.6	16	82.8	146.7	4.5	67.9	81.4	149.7	4.5	67.8	81.0	156.2	4.5	68.3	81.0	156.2	4.5	68.3
25	26.0	14	85.8	152.1	5.4	57.5	83.8	153.2	5.3	58.7	82.8	165.7	5.3	57.9	82.8	165.7	5.3	57.9
30	30.2	13	83.5	197.0	5.2	66.1	81.6	183.4	5.3	64.4	79.6	187.9	5.4	63.2	79.6	187.9	5.4	63.2
35	33.7	12	83.6	185.3	4.6	91.6	81.2	173.4	4.6	90.4	79.3	180.4	4.6	92.4	79.3	180.4	4.6	92.4
40	39.0	8	81.8	167.2	7.3	62.7	78.8	160.2	7.3	62.2	77.3	167.7	7.3	62.4	77.2	168.0	7.3	61.8
45	46.4	12	84.8	154.9	5.3	71.2	81.1	150.4	5.3	72.7	79.6	167.9	5.2	73.5	78.7	169.9	5.1	76.3
50	49.9	17	85.1	156.4	4.2	76.0	81.3	151.9	4.2	75.3	79.3	170.3	4.2	74.4	78.0	171.9	4.2	73.9
55	55.0	22	85.3	181.7	4.1	58.1	81.4	168.3	4.2	57.0	77.9	183.4	4.2	55.9	76.1	180.9	4.2	56.9
60	60.7	24	84.3	211.5	4.3	48.9	80.5	188.9	4.3	48.8	75.4	195.5	4.3	48.7	73.8	189.3	4.3	48.9
65	64.0	24	82.7	240.6	3.6	68.1	79.8	209.5	3.6	68.0	73.5	207.3	3.6	67.9	72.6	200.1	3.6	68.4
70	68.3	15	82.8	251.7	4.8	65.2	80.0	213.2	4.8	64.5	73.4	209.7	4.8	64.9	72.5	202.3	4.8	65.8
75	75.4	10	86.7	245.7	7.3	45.8	81.3	188.6	7.2	46.9	75.7	197.6	7.2	46.8	73.7	192.0	7.3	46.0
80	79.1	9	80.9	292.0	6.9	58.1	81.0	232.5	6.9	57.0	73.5	221.4	6.9	57.0	72.5	216.0	6.9	56.8
85	83.4	5	81.0	298.2	10.2	56.9	81.1	230.5	10.3	56.3	73.5	220.5	10.2	56.7	72.1	216.1	10.2	57.6
90	91.4	8	87.6	324.9	3.9	203.4	80.8	185.8	3.5	245.6	75.3	196.4	3.5	247.1	71.9	195.5	3.5	251.7
95	94.1	8	86.3	356.4	6.6	72.2	81.8	183.4	6.4	76.5	76.4	197.7	6.4	76.3	73.0	195.8	6.4	76.3
100	100.2	6	80.3	32.6	12.0	33.4	85.1	144.5	11.5	36.3	81.7	198.3	11.5	36.3	78.1	190.4	11.4	36.5
105	104.6	4	82.4	23.7	24.2	17.1	81.2	173.5	24.7	16.5	76.8	191.5	24.6	16.5	73.0	191.3	24.7	16.5
110	110.8	7	78.1	9.2	8.9	49.1	82.1	203.8	8.7	51.9	75.4	208.8	8.7	51.7	72.5	206.1	8.7	51.8
115	116.4	13	76.5	19.6	2.2	346.5	79.7	186.2	2.5	278.4	74.7	194.6	2.5	281.3	70.9	195.5	2.5	280.3
120	120.1	13	77.0	11.9	2.9	205.9	76.5	193.5	3.1	178.5	71.2	194.2	3.1	178.6	67.4	197.2	3.1	178.3
125	122.8	10	76.8	14.2	3.8	165.7	75.7	192.4	3.5	193.5	70.5	192.5	3.5	193.6	66.7	196.1	3.5	193.8
130	130.9	4	71.9	18.8	7.8	139.7	77.4	195.2	7.0	172.8	71.9	196.5	7.0	173.8	68.2	198.7	7.0	174.3

Table 5. (continued)

			Antarctica				Europe				North America				Greenland			
Window	Age	*N*	λ (°N)	ϕ (°E)	A_{95}	*K*	λ (°N)	ϕ(°E)	A_{95}	*K*	λ (°N)	ϕ (°E)	A_{95}	*K*	λ (°N)	ϕ (°E)	A_{95}	*K*
135	134.3	5	71.8	18.5	6.0	165.6	76.8	190.	5.5	194.5	71.8	192.3	5.5	195.1	67.9	195.3	5.5	195.7
140	139.3	5	70.9	358	8.0	92.3	72.6	203.1	8.1	90.0	66.7	197.2	8.1	90.0	63.2	201.6	8.1	90.0
145	142	3	72.0	346.8	11.9	109.1	68.7	201.9	11.7	111.3	63.1	193.9	11.7	111.2	59.4	199.8	11.7	111.2
150	153.9	4	63.9	41.5	6.1	231.0	73.2	134.3	6.1	227.2	75.7	141.6	6.1	226.9	70.4	155.2	6.1	226.6
155	155.7	7	62.9	37.2	3.9	245.6	74.3	137.4	3.5	296.2	76.2	146.8	3.5	295.5	70.9	159.1	3.5	295.2
160	158.9	5	65.2	31.1	6.4	144.1	71.9	149.7	7.1	117.9	72.4	154.1	7.1	117.7	67.2	164.8	7.1	117.8
165	168	8	62.8	26.5	9.8	33.7	70.6	149.5	9.7	34.0	71.2	151.9	9.7	34.0	65.9	163.2	9.7	34.0
170	170.2	13	60.6	34.8	6.8	37.8	70.1	129.9	7.7	30.4	73.5	131.5	7.7	30.4	68.4	147.4	7.7	30.4
175	176.7	13	53.2	45.1	7.2	33.8	66.0	96.4	7.4	32.4	73.4	84.5	7.4	32.4	70.3	110.4	7.4	32.4
180	178.4	12	51.6	44.6	7.6	33.4	66.0	91.7	7.6	33.4	73.8	77.9	7.6	33.4	71.1	105.2	7.6	33.4
185	182.4	9	50.1	48.5	7.6	46.5	63.7	87.7	7.6	46.5	71.7	71.2	7.6	46.5	69.6	97.9	7.6	46.5
190	191.3	13	55.9	43.1	5.5	58.4	65.9	102.5	5.5	58.4	72.8	92.8	5.5	58.4	69.2	116.8	5.5	58.4
195	194.4	14	57.2	42.3	4.9	67.9	65.8	105.8	4.9	67.9	72.5	97.2	4.9	67.9	68.6	120.2	4.9	67.9
200	198.9	8	58.0	54.4	5.7	94.9	59.4	103.5	5.7	94.9	66.4	90.5	5.7	94.9	63.0	111.9	5.7	94.9

[a] Same as Table 4.

the 10 to 60 Ma poles, and ~4° shift of the 80 to 110 Ma poles. The 120 and 130 Ma poles agree, but the two paths diverge prior to 140 Ma, with a maximum difference of 14° at 170 Ma. Actually, when one takes into account the A_{95} uncertainties, only the 173–175 and 178 Ma poles fail to intersect. Altogether, the new BC01 African APWP returns on itself rather than forming an open loop in the 90–200 Ma interval.

4.2. Checking the Geocentric Axial Dipole Hypothesis

[30] The comparison between the 10 Myr and 5 Myr resolution APWPs is best described in the case of the plate with the fastest polar wander rates, i.e., India. This is done in a later section. However, before comparing the new and old versions of the synthetic APWP for other plates, we address the question of dipolarity of the past geomagnetic field. As recalled above, a significant quadrupole, on the order of a few percent of the axial dipole, has been identified in the mean geomagnetic field for the last 5 Myr [e.g., *Johnson and Constable*, 1997; *Carlut and Courtillot*, 1998]. In Figure 6, we have plotted all the poles from our database referred to a common site longitude. In each 20 Myr time window, all sites are related to a common longitude (taken to be 0), and all such frames are stacked from 0 to 200 Ma. When a mean pole is computed in each time window, a jagged path results (Figure 7). Poles tend to follow an erratic course, yet remaining most of the time in the hemisphere opposite to the one centered on the reference meridian. Of course, the angular distance from the pole is small (on the order of 2° on average) and the uncertainties are such that most 95% confidence intervals include the geographical pole. When a grand 200 Myr average is computed, the mean pole lies at λ = 88.6°N, ϕ = 176.5°E (A_{95} = 1.2°), i.e., on the far side of the reference meridian, 1.4 ± 1.2° away from the geographical pole. If taken at face value, this would imply a far-sided effect due to a persistent quadrupole on the order of 3% (±2%) of the dipole, i.e., somewhat smaller than the 5 Myr average. This translates to a maximum effect of 3° on inclination at the equator, and translates into a paleolatitude error of 1.5° at most when the axial dipole hypothesis is used. We conclude that there are indications in favor of a persistent quadrupole on the 200 Myr timescale, with an amplitude on the order of half the one obtained for the last 5 Myr. However, these values are not distinguishable from zero in any individual 10 or 20 Myr time frame (except at 52 and 59 Myr), and in any case the effect is small and on the order of contributions from other sources of paleomagnetic uncertainty. With the resolution we are able to achieve, these quadrupolar effects remain negligible and the geocentric axial dipole (GAD) hypothesis is clearly satisfactory on the timescales of interest to our study (10 to 200 Myr).

4.3. Description of Individual Plate APWPs

4.3.1. Africa

[31] We have already illustrated the main characteristics of the BC01 synthetic APWP in South African coordinates (using the 20 Myr sliding window) (Figures 1 and 5). The path can be described in terms of a succession of track segments and standstills, i.e., of episodic polar wander [e.g., *Briden*, 1967; *Gordon and Cox*, 1980; *Cox and Hart*, 1986; *Irving and Irving*, 1982]. Poles tend to cluster at 10–20 Ma, 90–100 Ma, 180–190 Ma and a sharp hairpin occurs at 140 Ma. These relative standstills and cusps separate tracks with rather fast and regular polar wander: 20–90 Ma, 100–140 Ma, 140–180 Ma.

4.3.2. Europe and North America

[32] The synthetic APWPs in European and North American coordinates share the same major features, related through the slow opening of the North Atlantic Ocean at the end of the Cretaceous (Figure 8a). A track from 10 to 50 Ma is preceded by a more complex path between 130–140 and 50 Ma, with a general change in trend. A previously undetected loop occurs between 50 and 110 Ma. It can in a way be taken to represent a standstill, but some of the features in the loop appear to be resolved by individual mean poles. In particular, the 52 and 59 Ma averages are statistically distinct. A problem comes from the fact that much of the loop overlaps in time with the Cretaceous Long Normal Superchron, during which oceanic spreading rates are assumed to be constant for lack of observable chrons. This introduces a decrease in the temporal resolution of the kinematic models which are used to transfer poles.

[33] There are distinct cusps at 140 and 180–190 Ma, as was the case for the African path. The overall shape of the Eurasian APWP between, say, 50 and 150 Ma confirms the loop which was one of the new, previously ill-recognized features uncovered in BC91. The loop appears a bit smaller

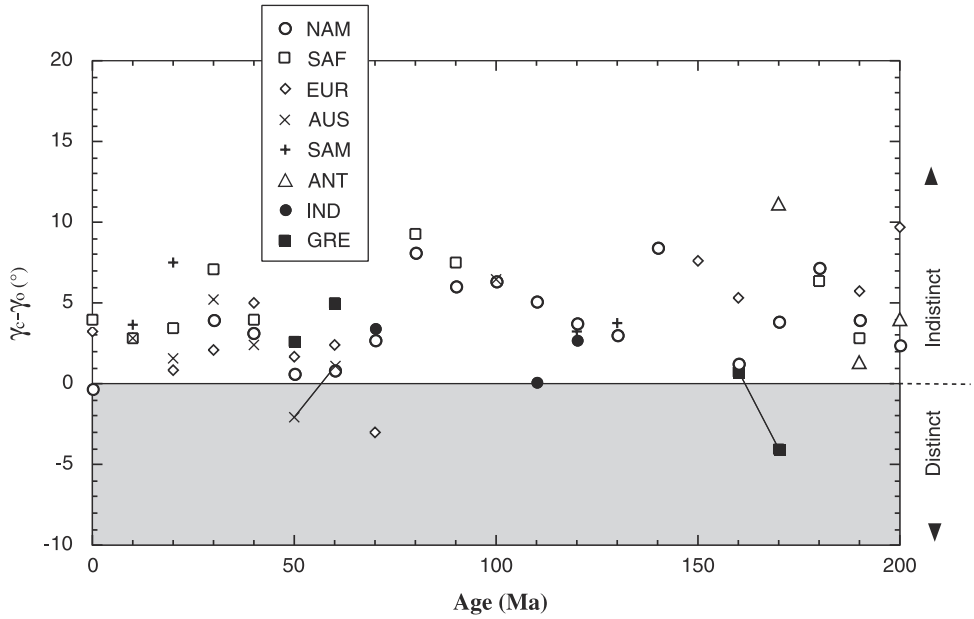

Figure 4. The *McFadden and McElhinny* [1990] test applied to each calculated mean pole for each plate versus the corresponding overall mean (synthetic) pole for the same 20 Myr time window as a function of age (the vertical axis corresponds to the calculated test parameter $\gamma_c - \gamma_o$). If negative (gray shaded zone), pole pairs are considered distinct at the 95% probability level. Two poles (AUS near 55 Ma and GRE near 165 Ma) fall in between rounded ages and can be assigned to either one of two synthetic poles (at 50 and 60 Ma and 160 and 170 Ma, respectively); hence two test points linked by a straight line segment are shown.

and may have a more complex structure than previously recognized. The timing of the so-called Cretaceous standstill [*Westphal et al.*, 1986; *Besse and Courtillot*, 1991] appears to be somewhat later: 60–110 Ma rather than 70–130 Ma. This loop was a significant feature used to analyze paleomagnetic data from mobile zones and large continental blocks in Asia [e.g., *Besse and Courtillot*, 1988, 1991; *Enkin et al.*, 1992]. Consequences in the changes in shape of the Eurasian APWP for such analyses are not explored further in this paper.

[34] Because most data on which the Jurassic segment of the NAM APWP could be based carried some amount of uncertainty (tectonic rotations for data from the SW United States, remagnetization on intrusions from the NE United States), *Courtillot et al.* [1994] proposed to transfer their available data from other continents to generate synthetic NAM APWPs. They discussed the effects of data selection and kinematic reconstructions. They concluded that the high latitude APWP of *Irving and Irving* [1982] was to a large extent vindicated, though with much reduced uncertainties at the 95% confidence level. On the other hand, the lower latitude paleomagnetic Euler pole-based path of *May and Butler* [1986], though on the edge of the confidence intervals, was not supported by the synthesized path. It is interesting to compare the path for North America from the present study with the earlier attempts by *Courtillot et al.* [1994]. Basically, the new path (Figure 8b and Table 4) vindicates the conclusions based on BC91. The 130–200 Ma segment of the NAM APWP remains at rather constant latitudes on the order of 70–75°N, with the mean A_{95} reduced from 7° to 5°. Reliable poles are now obtained at 140 and 170 Ma, due to the increased number of data, which were not sufficient in BC91. The main difference lies with the 200 Ma pole. *Van der Voo* [1990] emphasized that a pole transfer using the *Bullard et al.* [1965] fit led to North American and European APWP segments in better agreement during the Paleozoic and part of the Mesozoic. The problem is to understand when and how the change in configuration between the reconstruction based on the oldest seafloor data [see *Royer et al.*, 1992] on the one hand, and on the *Bullard et al.* [1965] fit on the other, was achieved. Our European database allows one to compute separate 185 and 190 Ma mean poles with three and five studies, respectively. The comparison between these two poles and a version of our master APWP from which European data have been removed is inconclusive at the 95% level, leaving this question still open, as already concluded by *Van der Voo* [1993].

4.3.3. South America

[35] As is well known, the SAM APWP is remarkable in that it displays very little polar wander (Figure 9a). Most poles have latitudes higher than 80°: South America has basically remained in the same position with respect to the geographical poles (i.e., spin axis) in the last 200 Myr. However, the path is ordered and shows small but resolvable features, such as a track from 200 to 180 Ma, a change in direction near 180 Ma, a track from 180 to 130–140 Ma and little motion since (with a real standstill between 50 Ma and the Present).

4.3.4. Australia, India, and Antarctica

[36] It is particularly informative to draw the three APWPs on Figure 9b. In BC91, the Indian APWP was shown only back to 120 Ma, and only two paleomagnetic poles for that plate (Deccan and Rajmahal Traps) were available; Australia and Antarctica had not been included in our previous analysis.

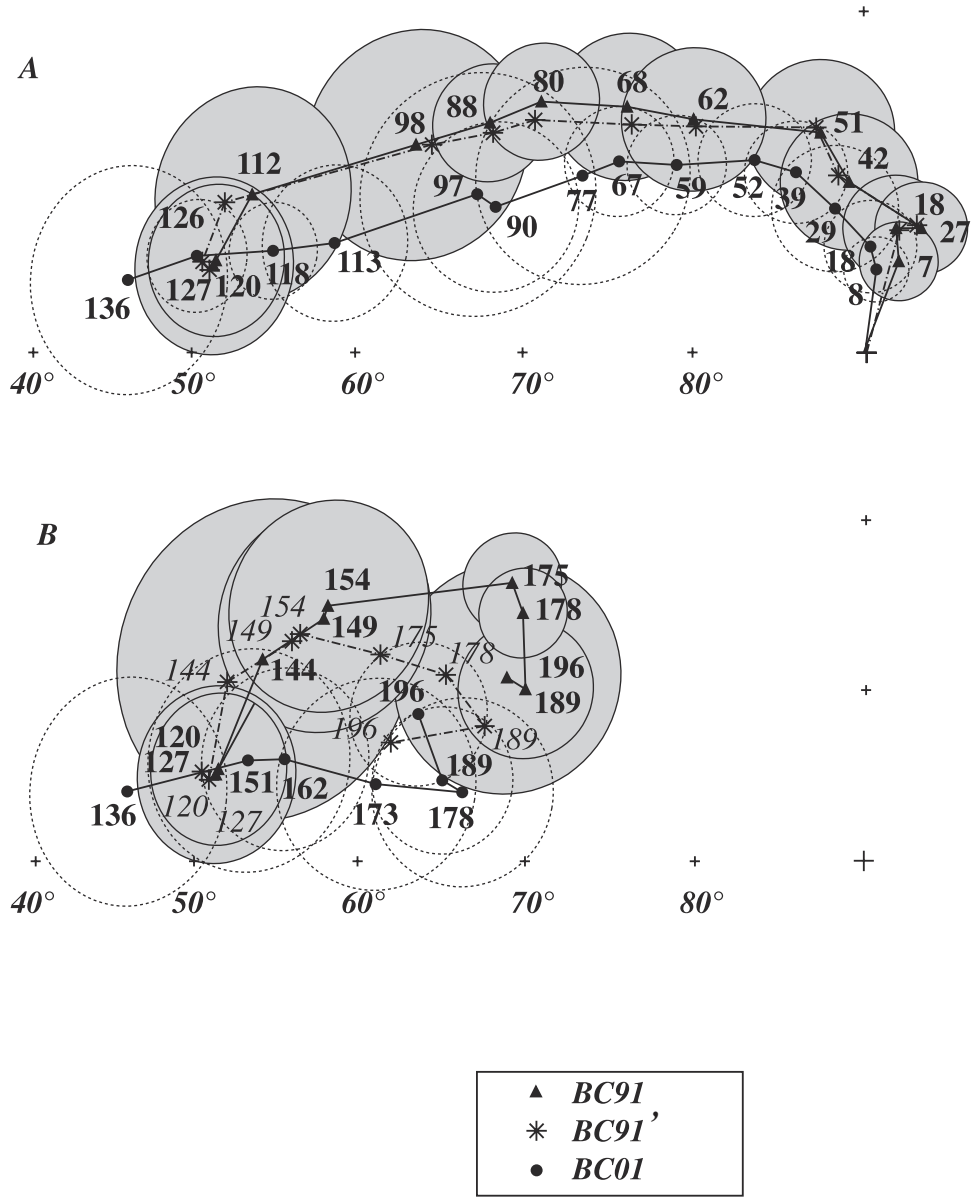

Figure 5. Comparison of three synthesized APWPs in South African coordinates with their associated 95% ellipses of confidence: triangles are for BC91 [*Besse and Courtillot*, 1991], dots for BC01 (this paper), and stars for BC91' (BC91 data transferred using the kinematics used in the present paper). (a) From Present to 140 Ma and (b) from 120 to 200 Ma. The ellipses of confidence for the BC91' path are not figured for more clarity. In Figure 5b, the age numbers in italic refers to the BC91'path. Ages are in Ma. Equal-area projection.

[37] The Indian path is the most elongated one, corresponding to the fastest average apparent polar wander velocity. Three phases (tracks) are clearly recognized from 180 to 130, 130 to 80–70 and 80–70 Ma to the Present. These are separated by a standstill (i.e., poles are in the joint intersection of their 95% confidence intervals) at 200–170 Ma, another one at 140–110 Ma and a directional change at 80–70 Ma. The classical rotation and northward motion of India are clearly outlined; the fast velocity (150 km/Myr) peaking between 70 and 50 Ma, and the slowdown after the India-Asia collision at 50 Ma are also seen. The 66 Ma Deccan Traps pole [*Vandamme et al.*, 1991], which is based on a very large number of data already used in our Indian selection of poles (and for that reason, not used in constructing the synthetic path) and very accurately dated falls only 1° away from the 67 Ma synthetic pole (Table 4), attesting to the validity of the data selection process, to the quality of the selected paleomagnetic data and plate kinematic parameters.

[38] Because of its fast polar wander rate, the synthetic APWP in Indian plate coordinates is the one for which the influence of improving time resolution from 20 Myr to 10 Myr moving averages is best displayed. This is shown in Figure 10, where only the 95% confidence circles for the 10 Myr APWP have been included for clarity. The mean poles are labeled with the mean age of the data they are actually based on (Tables 4 and 5). The excellent agree-

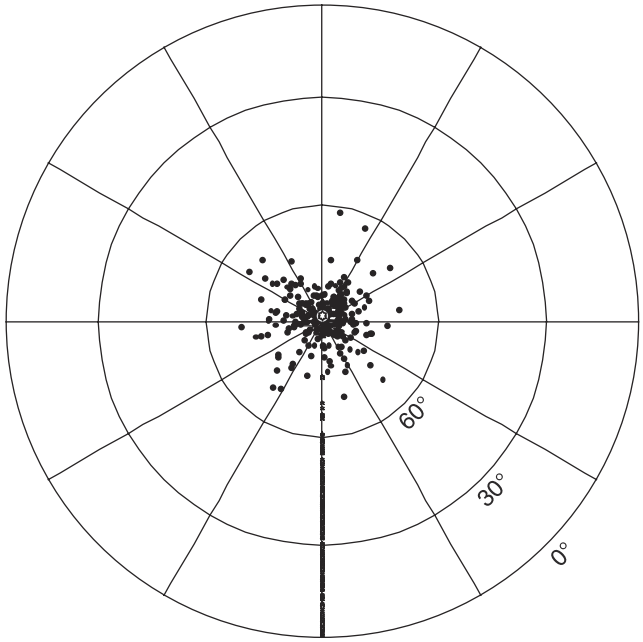

Figure 6. All poles from our database referred to a common site longitude. Open star and 95% confidence circle: grand 200 Ma average. Inclination alone allows only the determination of small circles of equal paleo-colatitude on which the pole must lie.

ment between the two curves is obvious. Of course, some features are more readily apparent in the higher resolution curve, such as the slowdown at 55 Ma, compatible with an early collision age for India versus Asia [e.g., *Patriat and Achache*, 1984; *Jaeger et al.*, 1989], or the sharper reorientation in the track at 75–80 Ma. The 10 Myr resolution pole at 100 Ma (nominal age 100.2 ± 4.1 Ma, with 6 data) and the corresponding 20 Ma resolution pole (nominal age 97.6 ± 5.8 Ma, with 12 data) are both well within the intersection of their respective 95% confidence circles (10.9 and 7.3°). The small loop in the 10 Myr APWP based on four mean poles between 130 and 142 Ma is not resolved given A_{95} between 6 and 12°; all are within less than 5° from the 20 Ma resolution pole at 140 Ma (nominal age 136.8 ± 5.4 Ma) which has an A_{95} of 6.4°. At the older end of the curves, the 10 Myr resolution poles at 194 and 199 Ma and the 20 Myr resolution pole at 196 Ma are fully compatible.

[39] In conclusion, the 20 Myr resolution curve captures all the essential features which can be found in the 10 Myr curve, and it is not expected that limiting our discussion to the former would run the risk of having missed any significant feature. The high-resolution curve also confirms the validity of the rough classification of APW periods into tracks and standstills.

[40] The Australian APWP (Figure 9b) displays almost the same track times and orientations, standstills and track changes as that for India until 70 Ma. Motion since 70 Ma is similar to that indicated by India (i.e., mostly northward motion follows after counterclockwise rotation) except it is three times slower between 80 and 50 Ma, and then accelerates a bit from 40 Ma onwards, in relation with the southward jump of the eastern branch of the South Indian Ocean ridge. After that time, Australia and India belong to the same plate.

[41] The Antarctic APWP (Figure 9b) again displays similar features prior to 70 Ma, with two standstills and two tracks, but since then, apparent polar wander is almost negligible, much like South America. The shapes of the three APWPs shown in Figure 9b are easily related one to the other as a function of the opening of ocean basins between plate pairs. The relative orientations of the relative velocity vectors and the respective rates of polar wander and plate motions combine in such a way that the respective influences of and relationships between the various parameters are readily apparent.

4.3.5. All Paths

[42] The succession of tracks, standstills, loops, and directional changes for all APWPs shows similarities and differences between the various continents. All paths begin with slow motion or standstill between 200 and 170–180 Ma and then turn into tracks which last until 140 Ma. A major re-organization occurs at 140 Ma, with AFR, EUR, NAM and SAM changing track direction, and IND, AUS, ANT entering a standstill. IND, AUS, ANT and SAM undergo a change at 110 Ma, but the other three plates do not. AFR, EUR, and NAM have a track ending near 100 Ma, and enter a standstill or loop. A 80 Myr change is common to IND, AUS and ANT; one at 40–50 Ma to AFR, EUR and NAM. Altogether, the 180–140 Ma track is the main feature which stands out to be common to all plates.

[43] A common succession of a fast (220–200 Ma, not documented in this paper) phase followed by a general

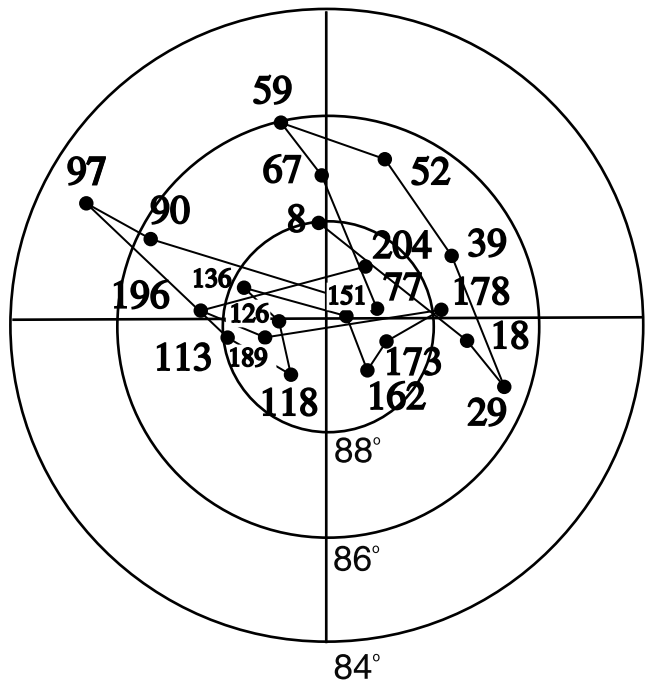

Figure 7. Mean poles computed in successive 20 Myr time windows, every 10 Myr, using the common site longitude poles of Figure 6. Full radial scale is 10° only. Notice the small angular distance of each mean from the pole (on the order of 2° on average); 95% confidence circles are not shown, for clarity; all but two include the geographical pole.

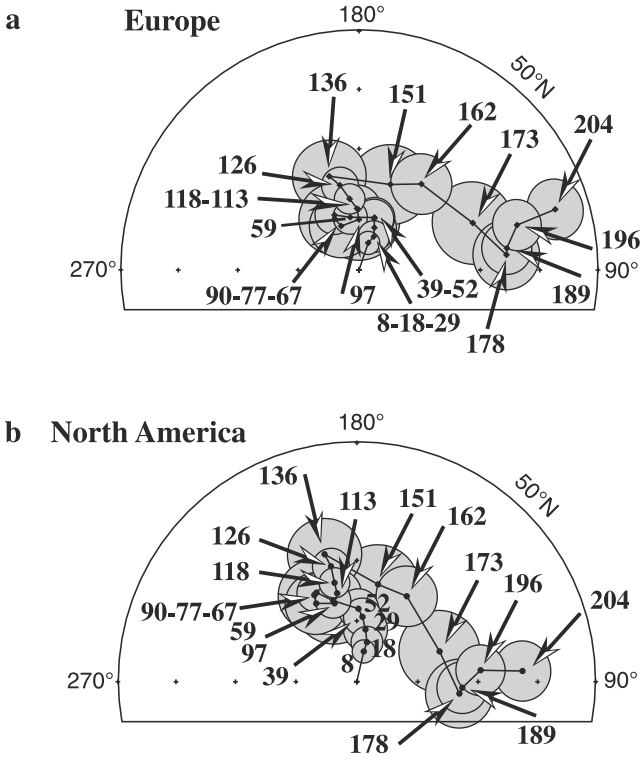

Figure 8. (a) Europe and (b) North American synthetic APWPs (data in Table 4). Each pole corresponds to a mean pole computed by using a 20 Myr sliding window. Equal-area projection. Ages are in Ma; the values shown are the actual mean ages derived from the data in the appropriate window.

standstill of Pangea at 200–180 Ma is followed by the breakup of Gondwana and the opening of the central Atlantic Ocean. An animated sequence derived from the APWP (www.ipgp.jussieu.fr/~besse/tpw_jgr01) shows a sequence of general rotations around 160–140 Ma. The next phase of breakup of Gondwana results in the 110–100 Ma events. The directional change of IND and AUS at 80 Ma does not show as a major event.

5. True Polar Wander

[44] As was previously done by *Livermore et al.* [1984], *Andrews* [1985], ourselves (BC91), and recently *Prévot et al.* [2000], we have attempted to combine apparent polar wander based on paleomagnetic data (paleomagnetic reference frame) with motions of hot spots with respect to lithospheric plates (hot spot reference frame) in order to derive true polar wander (TPW). Given the relative motions between the plates, the position of these plates with respect to the rotation axis (provided by paleomagnetic results under the GAD assumption) and the relative motions between the plates and a reference frame attached to the mantle (if such a frame can be found), TPW is defined as the motion of the mantle with respect to the rotation axis. The latter is defined by hot spots, which are assumed to form an array of fixed points that provides the mantle reference frame.

[45] A number of the assumptions made to determine TPW may of course be found erroneous, such as the assumption of hot spot fixity. This is a long debated subject [e.g., *Molnar and Atwater*, 1973; *Molnar and Stock*, 1987; *Tarduno and Gee*, 1995; *Steinberger and O'Connell*, 1998; *Di Venere and Kent*, 1999; *Koppers et al.*, 2001]. In their analysis, *Müller et al.* [1993] find that motions between individual hot spots in the Atlantic and Indian Oceans are less than a few km/Myr, i.e., close to an order of magnitude less than typical plate motion. These Indo-Atlantic hot spots therefore do form a relatively coherent frame for that vast part of the Earth's lithosphere (and underlying mantle) ranging from North America to India.

[46] The major improvement of the present analysis over that in BC91, where *Morgan*'s [1983] hot spot tracks on the African plate were used, is the use of the revised model of *Müller et al.* [1993], at least for the last 130 Myr. This model combines a number of advantages such as inclusion of hot spot tracks from AFR, NAM, SAM, IND, and AUS and the same updated plate motions by *Royer et al.* [1992] that we used in transferring the paleomagnetic data from one plate to the next in order to build the synthetic APWPs. Therefore, the kinematics and chronologies are compatible, potentially reducing significantly sources of errors that could have affected the BC91 analysis. Unfortunately, only two hot spot tracks are available (Tristan da Cunha and Meteor/New England) between 90 and 130 Ma, implying potentially larger uncertainties for that period.

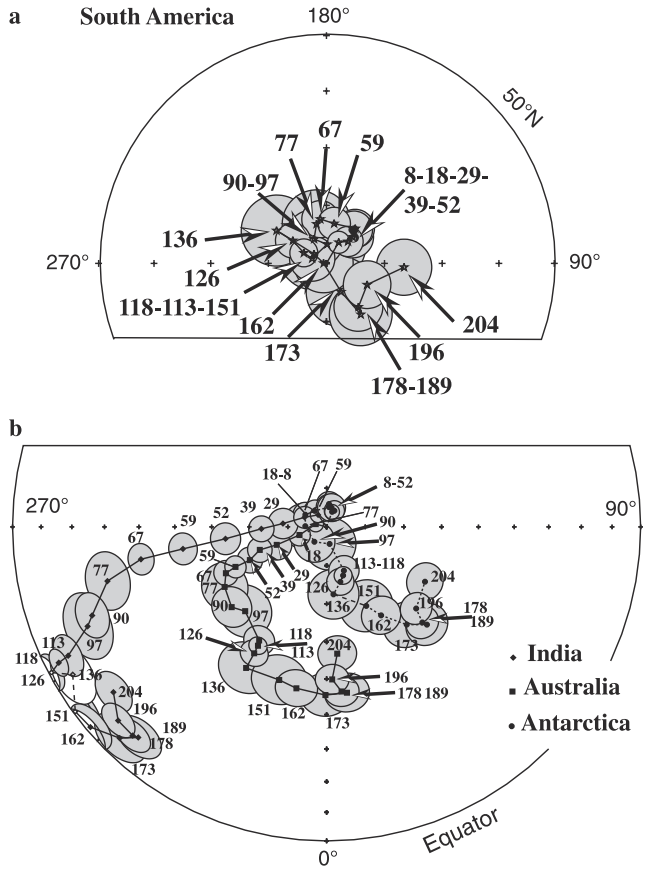

Figure 9. Same as Figure 8 for the (a) South American and (b) Indian, Australian, and Antarctic synthetic APWPs (see Table 4).

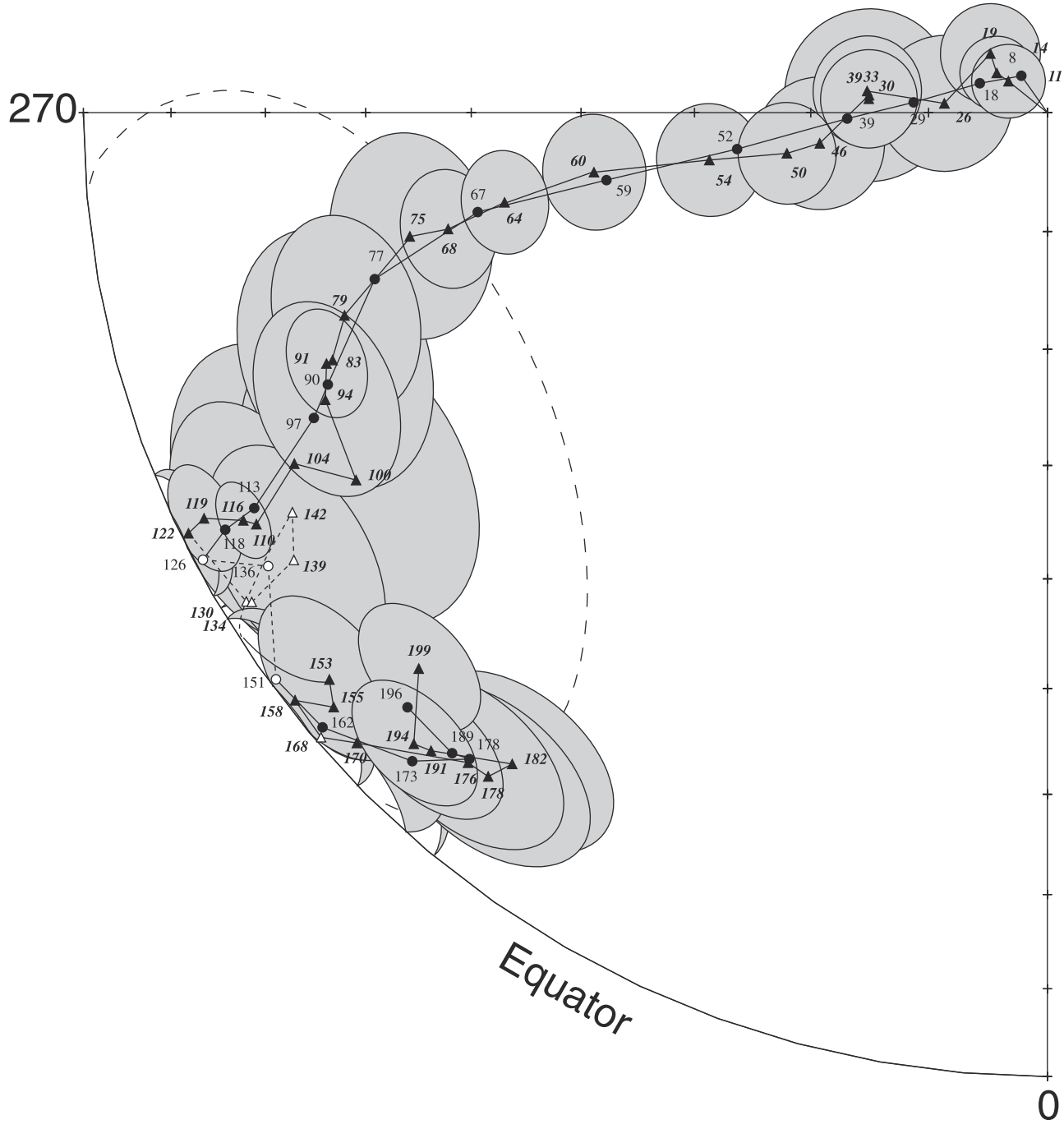

Figure 10. Comparison of two synthetic Indian APWPs. Triangles correspond to mean poles computed every 10 Myr using a 20 Myr sliding window (Table 4); dots correspond to mean poles computed every 5 Myr using a 10 Myr sliding window, and their associated 95% confidence ellipses are shown (Table 5). The dashed ellipse is the confidence interval of the ill defined 104.6 Ma pole. Ages are in Ma. Equal-area projection.

[47] The resulting TPW curve is shown in Figure 11, with 95% confidence circles, for the best (10 Myr) time resolution available (Figure 11a) and for the 20 Myr time resolution (Figure 11b) (also see Table 6). Points are shown every 5 Myr (10 Myr) and every other point is statistically independent. *Besse and Courtillot* [1991] compared BC91 TPW to two previous determinations by *Livermore et al.* [1984] and *Andrews* [1985], and we refer the reader to their Figure 3. In Figure 12, we compare BC91 (20 Myr resolution), the new BC01 curve of Figure 11a, and that obtained by *Prévot et al.* [2000].

[48] The first 11 points of BC01 in Figure 11a, corresponding to the period 0–55 Ma are all in the same quadrant, between 4 and 9° away from the present rotation pole, with 95% uncertainties ranging from 2 to 7°. They are not statistically distinct from each other and therefore could correspond to a standstill. A mean position can be calculated from all (102) data points in that time window: it is

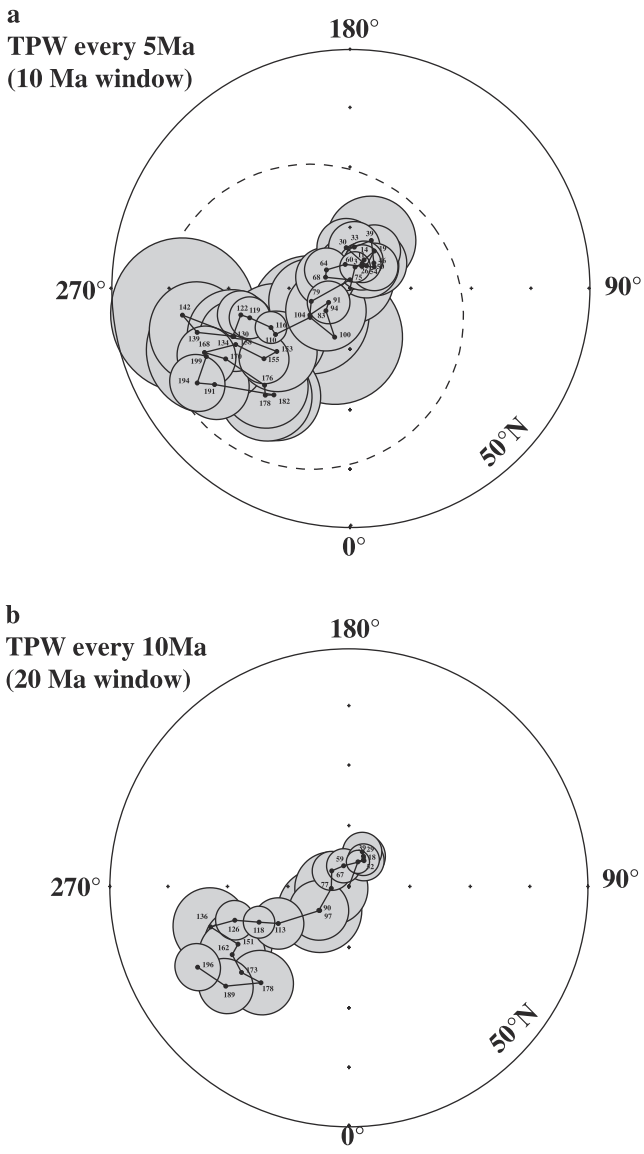

Figure 11. True polar wander paths (TPWP) deduced from the hot spot model of *Müller et al.* [1993] going from the Present back to 130 Ma, and that of *Morgan* [1983] going from 130 back to 200 Ma, with associated 95% confidence ellipses (shaded light gray). (a) For 10 Myr sliding window. The dashed ellipse is the confidence interval of the 104.6 Ma pole; (b) for 20 Myr sliding window. Ages are in Ma and correspond to the actual mean age of the data in the corresponding window. Data from Table 6.

found to lie at 85.1°N, 153.3°E (A_{95} = 1.5°), significantly displaced from the pole. The youngest pole at 5 Ma (mean age 3.0 ± 2.4 Ma) is at 86.4°N, 166.8°E (A_{95} = 2.5°), also significantly displaced from the pole but identical to the 55 Ma overall mean. It seems that TPW may have been negligible for an extended period of about 50 Myr, but accelerated a few Myr ago, with a velocity on the order of 100 km/Myr. Actually, the TPW path zigzags around the pole with no clear track as early as 75 Ma. There is another clustering of data points from 79 to 104 Ma, then the pole jumps to a different location, which is well constrained by the 116 Ma pole. The 95% confidence intervals of the 100 and 110 Ma poles are too large to outline with certainty the details of the track which is followed. The track extends to 142 Ma, when it turns back on itself. The path back to 200 Ma is again rather jagged although there is a tendency to drift away from the current pole. When 20 Myr time windows are used (Figure 11b), the path becomes somewhat smoother and a succession of a standstill at 160–130 Ma, a circular track from 130 to 70 Ma, and a standstill at 50–10 Ma follow each other. The true polar wander rate between 130 and 70 Ma averages 30 km/Myr. The BC91 TPW curve was somewhat smoother, with a large track between 50 and 120 Ma, in part because it was based on 20 Myr averages. However, differences between the two are of second order, given the uncertainties. TPW amplitude was smaller in BC91, with the same general features (tracks and sandstill) from Present back to 110 Ma, with maximum differences of order 3–4° in position between 70 and 90 Ma. On the other hand BC91 had a 120–150 Ma loop (or cluster) up to 8° away from the new BC01 path.

[49] It is interesting to compare the new BC01 TPW curve with that recently derived by *Prévot et al.* [2000]. The main difference between the two studies lies in the fact that

Table 6a. True Polar Wander Path for 10 Myr Sliding Window[a]

Age, Ma	*N*	λ(°N)	ϕ(°E)	A_{95}	*K*
3.1	30	86.3	172.2	2.6	105.2
11.9	21	85.5	153.7	3.1	107.3
14.8	24	84.9	151	3.2	85.1
19.6	16	82.5	143.7	4.6	67.1
26	14	85.4	143.9	5.3	58.5
30.2	13	83.6	185.3	5.2	65.9
33.7	12	83.5	172.7	4.6	90.4
39	8	81.4	156.1	7.2	63
46.4	12	84.3	136.7	5.4	70.1
49.9	17	84.7	134.2	4.1	76.5
55	22	85.8	154.9	4.1	58.2
60.7	24	86	191.2	4.3	49
64	24	85.1	232	3.6	68.7
68.3	15	85.6	245.7	4.9	63.4
75.4	10	89.4	154.6	7.3	46.1
79.1	9	83.1	300.3	6.9	57.6
83.4	5	82.1	303.7	9.7	63.3
91.4	8	85.8	303.7	3.5	247.6
94.1	8	84.6	313	6.6	72.4
100.2	6	81.6	342.4	11.1	38.4
104.6	4	81.9	306	25.2	15.8
110.8	7	75.5	301.7	8.3	56.6
116.4	13	75	296.7	2.7	248.1
120.1	13	72	286.6	3.2	172.3
122.8	10	71.4	284.6	3.5	194.5
130.9	4	69.1	292.4	7.6	148.9
134.3	5	69.3	292.6	5.7	180
139.3	5	63.7	286.2	8.1	89.5
142	3	61.9	279.1	12.3	100.9
153.9	4	74.1	310.7	6.6	196.1
155.7	7	71.8	309.2	4.1	214.3
158.9	5	69	296.2	7.7	100.5
168	8	63.7	293.8	9.8	33.7
170.2	13	66.4	299.5	6.6	40.5
176.7	13	68.7	318.6	7.1	34.9
178.4	12	67.5	321.6	7.6	33.4
182.4	9	68.4	324.5	7.6	46.5
191.3	13	62.4	305.4	5.7	53.6
194.4	14	60.2	301.8	4.6	74.8
198.9	8	63.5	296	5.6	100.4

[a] Apparent polar wander path for global (Indo-Atlantic) hot spots for the last 200 Myr.

Table 6b. True Polar Wander Path for 20 Myr Sliding Window[a]

Age, Ma	*N*	λ(°N)	ϕ(°E)	A_{95}	*K*
3.1	30	86.3	172.2	2.6	105.2
8.3	54	85.7	161	2	95.5
18.9	38	85	149.5	2.7	76.4
29.5	23	84.7	151.3	3.8	66.4
40	24	84.1	157	3.4	79.8
52.2	31	85	151.7	3.4	60
59.7	45	86.4	196.3	2.8	58.8
67.3	34	86.4	229.4	3.2	60
77.9	14	87.1	291	6	45.4
90	13	83.7	308.6	4.9	73.6
97.6	12	83.7	309.5	6.9	40.7
113.6	17	76.7	298	4.5	64.6
119.1	20	73.6	291.8	2.6	164
126.4	14	70.5	287	2.9	183.1
136.8	7	66.2	286.3	6.3	93.1
151.6	10	69.4	297.5	5.6	74.7
162.3	15	67.7	300.3	5.5	49.2
173.4	21	67.3	308.7	5.8	31.4
178.8	18	68.5	317.6	5.3	43.1
189.7	23	63.8	309.1	4.5	46.1
196.7	19	61.4	298.5	4	71.8

[a]Apparent polar wander path for global (Indo-Atlantic) hot spots for the last 200 Myr.

Prévot et al. use only paleomagnetic data from magmatic rocks and restrict themselves to basalts and andesites, or intrusive rocks with a similar composition. Their selection criteria were at least 10 sites (versus our 6) with at least 5 samples per site (versus our 6), the rest being similar to ours. Also they rejected data with potentially insufficient averaging of secular variation (K > 100). Their final database contains 118 poles, i.e., less than half of ours. The TPW they obtain is in general similar to ours (Figure 12). However, their 95% uncertainties (not drawn in their figure) are very large because of the small number of data points in most time windows. Like us, they find a succession of episodes, with a long and faster track separating two standstill periods. The most intriguing result they obtain is a phase of very fast wander culminating around 115 Ma, when 20° of polar wander take place at velocities in excess of 500 km/Myr, i.e., more than ten times faster than the mean rate we obtain on the track from 130 to 60 Ma. This result is based on two sets of individual poles dated around 100 and 120 Ma, and more specifically to the recordings around 115 Ma provided by South African kimberlites (114 to 118 Ma). It so happens that our database provides a sequence of rather well determined poles, particularly at 90 Ma (A_{95} = 4.9°; N = 13 poles) and 119 Ma (A_{95} = 2.7°; N = 20 poles). The angular difference is 10.0 ± 5.5° and the corresponding polar wander rate in this 28 Myr period is on the order of 40 km/Myr. We can attempt the same comparison between the 119 Ma pole and a 114 Ma pole (A_{95} = 4.2°): the angular difference is 3.2 ± 6.5° and is not resolvable. We therefore find no support for the episode

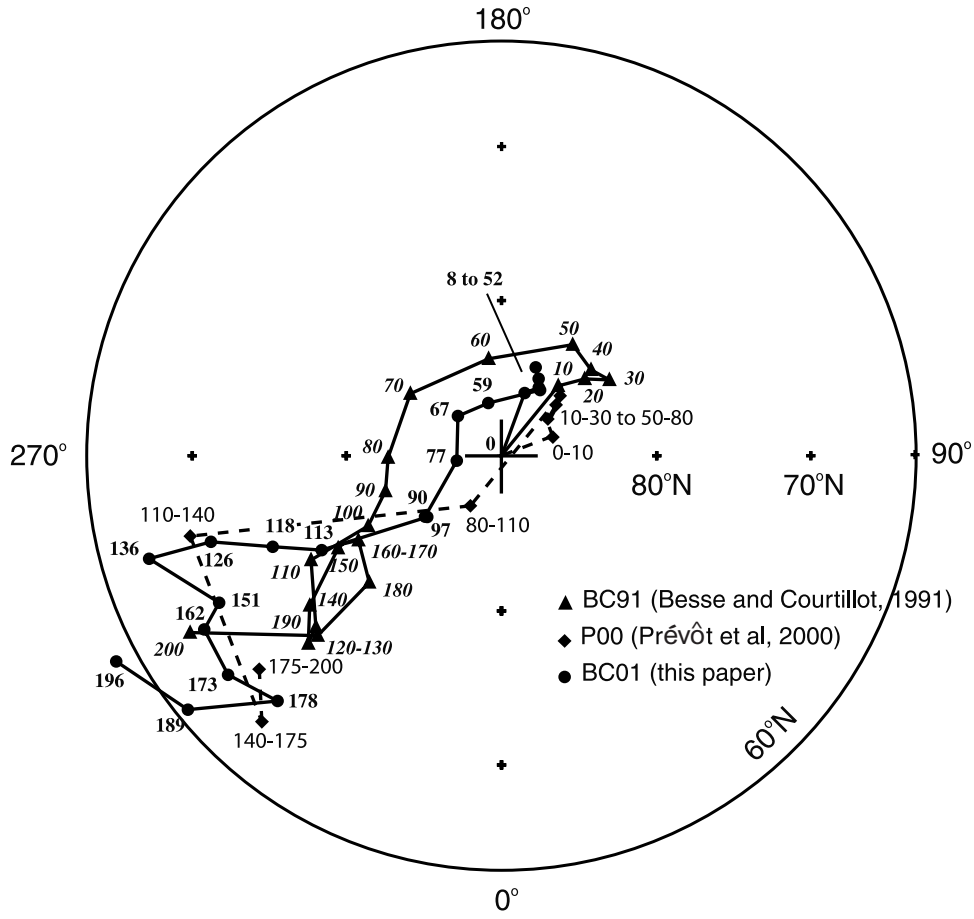

Figure 12. Comparison between three TPW Paths (95% confidence intervals not shown for clarity): dots, BC01 (this paper); diamonds and dashed line, *Prévot et al.* [2000]; and triangles, BC91 [*Besse and Courtillot*, 1991]. Crosses are at 10° intervals (see also Figure 11 and Table 6b).

of super fast TPW suggested by *Prévot et al.* [2000]. As stated by *Hargraves* [1989, pp. 1851, 1852] in his analysis of the dating of the 114 and 118 Ma kimberlites in South Africa, "it should be pointed out that accurate radiometric dating of these bodies is difficult" and "inconsistencies between the sequence of apparent pole positions and the available radiometric ages may in part be due to uncertainties in the age." The 114 Ma pole belongs to a 118–142 Ma petrochemical group, and the 114 Ma pole belongs to a distinct 83–114 Ma group. According to *Hargraves* [1989] "There is no clear pattern of migration with age" and "if it is argued that identical poles mean identical emplacement and magnetization age, then…the detailed validity of some of the radiometric ages must be suspect." The remarkable hypothesis of Prévot et al. is therefore hardly supported by such uncertain data. Actually, *Prévot et al.* [2000] average their data in four subsets (0–80, 80–110, 110–140, and 140–200 Ma) in order to reduce uncertainties. At that level, our two determinations are in good agreement, but evidence for any fine scale behavior or superfast episodes is lost.

6. Discussion

[50] The 10 and 20 Myr resolution TPW curves of Figure 11 provide our current best estimates of true polar wander over the last 200 Myr. We confirm earlier findings [e.g., *Andrews*, 1985; *Besse and Courtillot*, 1991] that true polar wander appears to be episodic in nature, with periods of (quasi) standstill alternating with periods of faster TPW. The typical duration of these standstill periods in on the order of a few tens of millions of years (50 Myr). Typical polar wander rates during fast tracks are on the order of 30 km/Myr. Also, because of all the uncertainties in models of hot spot kinematics prior to 130 Ma (and even possibly prior to 90 Ma), we feel it is not safe to place too much weight on behavior prior to that time. The major event since then is therefore the end of the 130 to 60 Ma period of relatively fast polar wander, with a standstill (i.e., no or little TPW) from 50 Ma (actually because of larger 95% confidence circles, possibly 80–50 Ma) to 10 Ma. However, uncertain, evidence for the fact that Earth emerged from that standstill to enter a new period of fast polar wander in a different direction 10 Myr ago (3 Ma at the higher resolution; see previous section) is particularly interesting. That period would then still be going on. Actually, the inferred rate and azimuth of this recent phase of accelerated TPW are compatible with the historical values based on direct measurements: between 1900 and 1990, the axis of rotation has been moving at a rate of 135 km/Myr toward eastern Canada (281°E; arrow on Figure 13 from *Hulot et al.* [1996]).

[51] A legitimate concern regarding the above conclusions is due to the fact that the analysis is not truly global, in that it fails to encompass the Pacific plate. *Petronotis and Gordon* [1999] have compiled an APW path (nine poles from 125 to 26 Ma) for the Pacific plate, with four poles based on the analysis of skewness of ocean crust magnetic anomalies, three on seamount magnetic anomaly modeling [*Sager and Pringle*, 1988] and two unspecified. Using the Pacific plate versus hot spot kinematic model of *Engebretson et al.* [1985], we have determined a corresponding 125 to 26 Ma "Pacific hot spot only" TPW curve (Figure 13). In

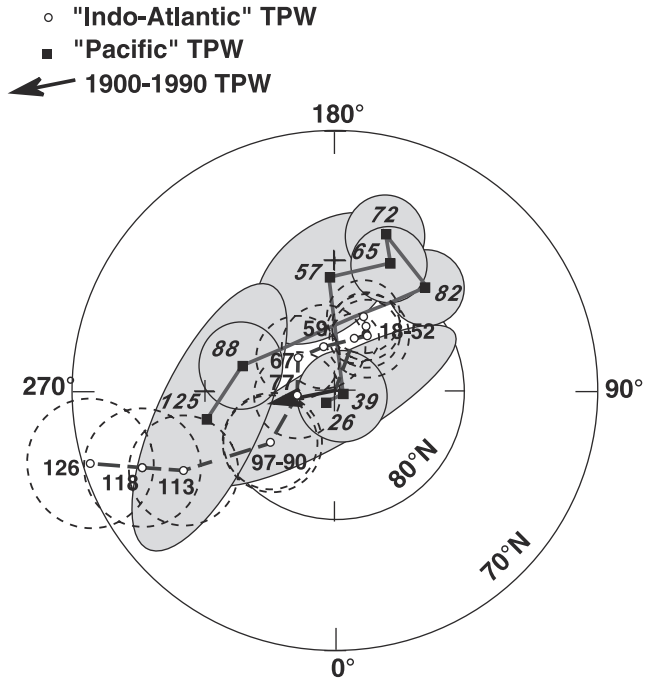

Figure 13. Comparison between the "Indo-Atlantic" (open dots and dashed line; this paper) and "Pacific" (squares and solid line) TPW Paths. The Pacific TPW is based on the Pacific APWP of *Petronotis and Gordon* [1999] and the plate/hot spot kinematic model of *Engebretson et al.* [1985]. The arrow shows the mean polar motion between 1900 and 1990 [after *Hulot et al.*, 1996].

that sense, the TPW estimate derived in this paper could be termed an "Indo-Atlantic" TPW. The "Pacific" and "Indo-Atlantic" TPW curves are compared in Figure 13. This comparison is interesting because the data sets they are based on are entirely different and independent. Despite some significant differences to which we return shortly, it is worth emphasizing that the two curves are similar in shape (tracks, amplitudes, azimuths), particularly the 300° longitude trending track from 130 to 70 Ma, though the two are offset (in the same general direction) by about 7°. More precisely, the confidence intervals intersect (though points are not in the intersection) near 125, 90, 60, 40 and 30 Ma. The main differences occur near 80 and 70 Ma: the 82 and 65–72 poles derived from *Petronotis and Gordon* [1999], and our poles at 77 and 67 Ma (which have moderate uncertainties), are clearly distinct.

[52] We emphasize that there are ongoing debates on the validity of the data used by *Petronotis and Gordon* [1999] to construct their Pacific APWP, and also on the question of fixity of Pacific hot spots with respect to each other and to the Indo-Atlantic hot spots. For instance, *Tarduno and Cottrell* [1997] have determined the paleolatitude (based on inclination-only data from cores) of the 81 Ma old Detroit Seamount, which is part of the Emperor chain, not far from its northern termination in the Kuril Trench. The paleolatitude (36.2 + 6.9/−7.2°) is distinct from that based on the 81 Ma pole of the Pacific APWP [*Sager and Pringle*, 1988; *Gordon*, 1983] which is on the order of 20°N. *Tarduno and Cottrell* [1997] exclude the possibilities of inadequate sampling of secular variation, bias due to unre-

moved overprints or off-vertical drilling. They point out the uncertainties encountered when building an APWP for an oceanic plate, such as the Pacific, solely from inversions of magnetic surveys over seamounts and/or analysis of skewness of marine magnetic profiles. *Petronotis and Gordon* [1999] evaluated the quality of their own skewness data, which they rank from A (best) to D (worst). The uncertainty in the 73Ma mean pole based on A quality data is 3 to 4 times larger than that of the mean based on all data (which they prefer). Yet the A quality mean pole is compatible, due to its large uncertainty, with the coeval 72 Ma pole of *Sager and Pringle* [1988]. It is therefore not clear that the conclusion of *Petronotis and Gordon* [1999] (namely, that the two are significantly different, when all data from A to D quality are used) can be accepted.

[53] Following several authors [e.g., *Parker et al.*, 1987; *Parker*, 1991], *Di Venere and Kent* [1999] argue that the reliability of the Pacific paleopoles based on either modeling of seamount magnetic anomalies or determination of skewness of marine magnetic anomalies should be considered suspect. They recall that both are prone to numerous biases and could yield errors in excess of 10° in the position of the mean poles derived from them.

[54] Let us now review briefly the question of hot spot fixity. *Norton* [1995] has suggested that the famous 43 Ma Hawaiian bend was actually a "nonevent," i.e., indicated a change in motion of the Hawaiian hot spot with respect to the mantle rather than a change in Pacific plate motion. *Koppers et al.* [2001] have tested the fixed hot spot hypothesis for Pacific seamount trails. They use seamount locations to first determine stage Euler poles, which they then test against observed $^{40}Ar/^{39}Ar$ age progressions. The stages tested are 0–43, 43–80 and 80–100 Ma. Koppers et al. find that the 0–43 Ma Hawaiian and Foundation seamount trail pair is the only one compatible with the fixed hot spot hypothesis. The 0–43 Ma Louisville/Hawaii, 43–80 Ma Emperor/Louisville and 80–100 Ma Magellan/Musician trail pairs would all require relative motions of order (or in excess of) 10 km/Myr. The 43–80 Ma Emperor/Line pair shows particularly large discrepancies, requiring motions of at least 30 km/Myr. However, we may note that the notion of stage poles does require minimum knowledge on the ages of the seamount trails being fitted, and therefore the determination of a geometrical stage pole is not strictly independent from age information. Koppers et al. also publish, but do not discuss, stage poles going back to 140 Ma. Altogether, four out of these six stage poles correspond to durations of only 10 to 20 Myr and the notion of a stage, with regard to dating uncertainties, becomes fuzzy. The authors emphasize that uncertainties in age progression may not entirely reflect true geological uncertainties, such as prolonged volcanic activity, rejuvenation by younger hot spots and uncertainties in location of hot spot (e.g., volcano hysteresis or hopping, control by lithospheric faults and structures). On the basis of careful analysis of 14 Pacific seamount tracks, using updated age determinations and bathymetry, *Clouard and Bonneville* [2001] show that these Pacific seamounts are created by different processes, most being short-lived and certainly not related to deep-mantle phenomena. Only the Hawaii and Louisville chains qualify as long-lived hot spots that can be robustly tested for fixity. We conclude that inter-hot spot motions of order 10 km/Myr (but not necessarily much more) of (the major) Pacific hot spots are a distinct possibility.

[55] *Di Venere and Kent* [1999] have addressed the problem of relative motion between the Pacific and Indo-Atlantic groups of hot spots. Though they demonstrate that some motion must have taken place between West and East Antarctica, based on geological observation and paleomagnetic data, they conclude that this motion cannot account for more than 20%, and possibly as little as 4% of the 14.5° offset between the observed and predicted positions of the 65 Ma Suiko seamount on the Emperor continuation of the Hawaiian hot spot track. They also discuss the integrity of the Pacific plate and the role of missing plate boundaries and errors in kinematic plate circuits, and find that they play a small role. DiVenere and Kent conclude that most of the apparent motion between the two main groups of hot spots is real, with an average drift of about 20 km/Myr since 65 Ma.

[56] Despite criticism on the quality of skewness data and seamount poles, which have strong bases, and increasing evidence that there can have been ~10 km/Myr motion between major individual hot spots or hot spot groups, we find the first-order agreement between the *Petronotis and Gordon* [1999] Pacific and our Indo-Atlantic TPW curves shown in Figure 13 quite remarkable. We therefore propose that our BC01 curve can be considered as a good first-order estimate of global TPW and that the frame of reference based on the surface traces of the major hot spots deforms only slowly, slower than plates and plate boundaries move with respect to each other. In that sense, these hot spots can be used as a frame of reference for the underlying mantle, regardless of their dynamics and depth of origin. Hence TPW appears to be a truly global phenomenon, with tracks, cusps, standstills, and more generally amplitudes and azimuths which are now reasonably well determined. *Cottrell and Tarduno*'s [2000] proposal that TPW has not exceeded 5° for the last 130 Myr is not vindicated.

[57] We now turn to evidence for episodes of fast to superfast TPW, which have been proposed by a number of authors. With due caution and suggestions of alternate explanations, *Petronotis and Gordon* [1999] see possible fast polar wander at 80–70 Ma. *Sager and Koppers* [2000] reexamined the 130–40 Ma segment of the Pacific APWP based on poles derived from magnetic anomaly modeling of $^{40}Ar/^{39}Ar$ dated seamounts (and only seamounts, with no skewness data) and concluded that a rapid TPW episode (300 to 1100 km/Myr) occurred in 2 to 5 Myr at about 84 Ma. The back and forth motion on Sager and Koppers' Pacific APWP between 73 and 117 Ma, and even more so on their TPW curve, are uncomfortable features that could well be linked to problems in data significance and statistical robustness. The 84 Ma motion, between the remote yet quasi-coeval poles 84W and 84E, in entirely canceled by previous motion from 93 to 84(W) Ma, and subsequent motion from 84(E) to 73 Ma (i.e., the 73 and 93 Ma points are not far from each other). Taken at face value, Sager and Koppers 84W and 84E poles would lead to TPW velocities in excess of 500 km/Myr, whereas the 93 and 73 Ma poles lead to values on the order of 50 km/Myr. Very recently, *Cottrell and Tarduno* [2000] have re-analyzed the data on which Sager and Koppers base their 84 Ma episode of rapid TPW. In addition to pointing out modeling or magnetization uncertainties in

the seamount data, they test the TPW episode against the reference paleomagnetic record from the Umbrian Appenines (Italy) and conclude that the episode must be an artifact of spurious seamount data.

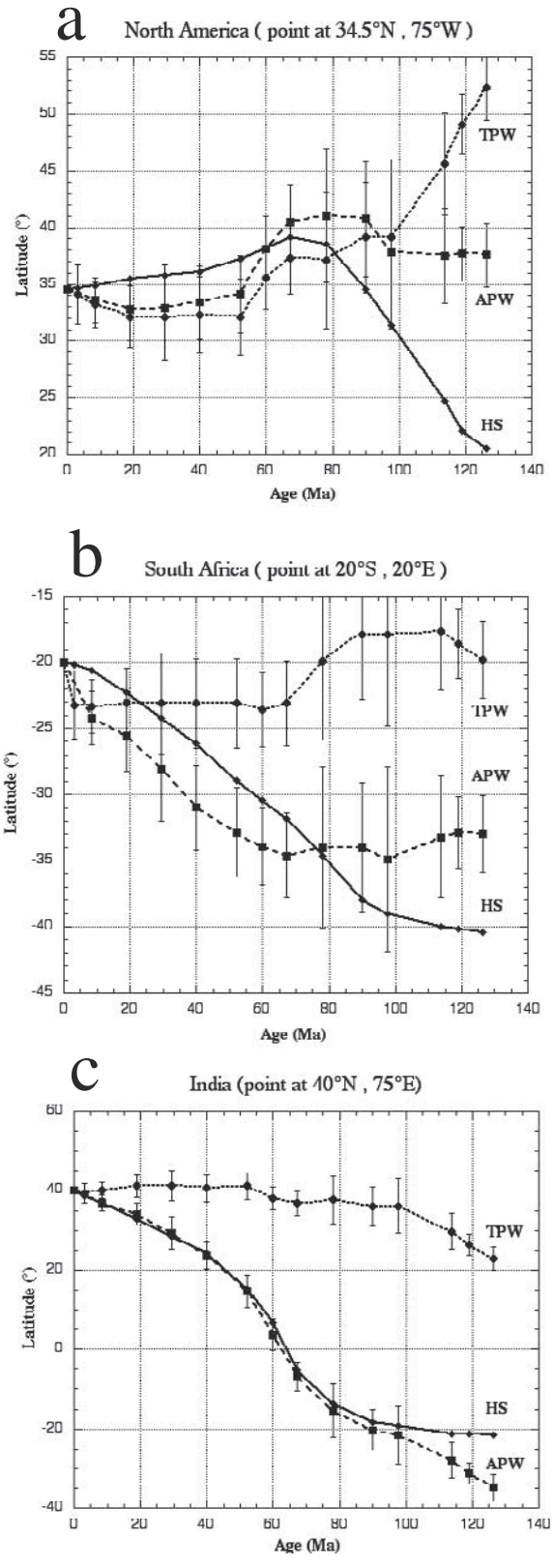

[58] We noted above the suggestion by *Prévot et al.* [2000] of the existence of an episode of superfast polar wander (500 km/Myr) at 114–118 Ma but concluded it was likely an artifact. Note that *Sager and Koppers* [2000] find no evidence for the *Prévot et al.* [2000] event, and vice versa. *Tarduno and Smirnov* [2001] argue, in a comment on the *Prévot et al.* [2000] analysis, that reliable, selected paleomagnetic data from mid-Cretaceous (90–125 Ma) granites from North America disagree with either paleolatitude predictions based on the hot spot reference frame or with the superfast (stepwise) TPW event of *Prévot et al.* [2000]. As correctly identified by *Camps et al.* [2001] in their reply, *Tarduno and Smirnov* [2001] failed to indicate that the three predicted "paleolatitudes" for North America are not independent. In Figure 14, we have plotted the "latitudes" predicted over the last 130 Myr (i.e., the time with better ocean kinematics and hot spot data) for test points respectively in North America, South Africa and India. Three latitudes are shown: "APW" is simply the paleomagnetic latitude predicted by our synthetic APWP, i.e., by the world paleomagnetic data set, when plate kinematics are integrated. We have seen that this was compatible with the very data originating from each respective plate or continent. Under the assumption of a GAD field, this is simply the geographical latitude. "HS" is the "latitude" predicted in a reference frame where the (Indo-Atlantic) hot spots would have remained fixed with respect to the rotation axis (i.e., no TPW). "TPW" is the latitude predicted by the TPW curve, i.e., motion of the point, as if it were attached to the hot spot reference frame, with respect to the rotation axis. The three latitudes (of which only the first, APW, corresponds to the true geographical latitude) are respectively linked to three rotations: APW is linked to Ω_1, the rotation of the plate with respect to the Earth's rotation axis, HS is linked to Ω_2, the rotation of the plate with respect to the hot spot reference frame, and TPW is linked to Ω_3, the rotation of the hot spot reference frame with respect to the Earth's rotation axis. The three motions are linked through the simple equation (1): $\Omega_1 = \Omega_2 * \Omega_3$. Therefore, any of the three latitudes can be derived from the two others, and they are by construction mutually consistent. In practice, we use APW and HS to deduce TPW. Figure 14a confirms that the three latitude estimates happen to be similar, and rather

Figure 14. (opposite) "Relative" latitudes calculated for three test points: (a) North America presently at 34.5°N, 75°W; (b) South Africa at 20°S, 20°E; and (c) India at 40°N, 75°E. In each case, three "latitudes" are given from Present back to 130 Ma: APW is the paleolatitude predicted from the synthetic APWP derived for that plate in the present paper; HS is the paleolatitude in the (Indo-Atlantic) hot spot reference frame, i.e., assuming no motion of the hot spots with respect to the rotation axis [*Müller et al.*, 1993]; TPW is the "paleolatitude," had the site remained fixed with respect to the hot spot frame of reference, while that frame moved with respect to the rotation axis, following our global TPW curve. The three estimates are linked since the first rotation (APW) is equal to the combination of the two others (HS and TPW; see text). 20 Myr averaging windows are used, and points are shown at their actual mean ages, with 2σ uncertainties derived from the 95% confidence intervals.

constant back to 80 Ma in North America. From 90 back to 130 Ma, the three estimates diverge. The observed paleolatitude (APW) remains constant, as has been long noted from NAM paleomagnetic data (and as is again emphasized by *Tarduno and Smirnov* [2001]). However, the HS and TPW estimates smoothly diverge in an opposite sense by roughly equal amounts. It so happens that they compensate each other in equation (1). Therefore, contrary to what is stated by *Tarduno and Smirnov* [2001], but in agreement with *Camps et al.* [2001], there is no disagreement between the three curves. We also find no evidence, as stated above, for the sudden jerk in TPW near 115 Ma, which would need to be compensated by an opposite, fortuitously coeval jerk in hot spot latitude. We note in passing that this agreement of the synthetic path with paleomagnetic data derived from granites somewhat alleviates worries on the quality of these data, as argued by *Tarduno and Smirnov* [2001].

[59] Figures 14b and 14c display similar results for points on the African and Indian plates, in order to show that the respective behaviors of the three latitude estimates of course depend on the distance and azimuth under which the APW and TPW paths are seen. In the Indian case for instance, TPW results in very little change in latitude, at least back to 100 Ma, and the APW and HS latitudes are virtually identical. This was shown from paleomagnetic data of the Reunion hot spot trace on the Indian and African plates during ODP leg 115 [*Schneider and Kent*, 1990a; *Vandamme and Courtillot*, 1990]. For the 100–130 Ma period, the HS latitude of India becomes more northerly than the APW latitude, whereas the reverse holds for South Africa. Such curves can be calculated for any point on any plate used in our database. They allow quick comparison of actual paleomagnetic data, predictions from the master synthetic APW, and values predicted from the hot spot or TPW curves (reference frames). Figure 14 serves to illustrate that the characteristics of these three curves depend very much on the location to which they apply.

[60] In conclusion, none of the several suggested superfast events is based on sufficiently robust sets of observations. It remains reasonable to assume that many of these features correspond to erroneous individual data or other sources of error. Only the recent phase of TPW since 10 Ma prompts us to accept that TPW velocities on the order of 100 km/Myr can be maintained over periods of millions of years, although we have no specific geodynamic explanation for this event (which some authors associate with deglaciation and rebound).

[61] Whether even faster velocities over shorter timescales actually occurred cannot as yet be considered as a strong constraint that should be modeled in numerical experiments. Studies of TPW and mantle dynamics have entered a new phase with the advent of flow models, where seismic tomography is used to infer 3-D maps of density heterogeneities that drive flow in the viscous mantle. For instance, *Steinberger and O'Connell* [1997] calculate the degree 2 nonhydrostatic component of the geoid and derive inertia perturbations on Earth over the last 60 Myr. Their results are in reasonable agreement with our earlier BC91 TPW estimates, though slightly larger. However, their model has smooth and regular TPW changes, rather than the episodic structure interrupted by standstills which we find. *Richards et al.* [1999] calculate polar motion for different Earth models. Interestingly, isoviscous mantle models predict TPW rates much larger than observed, and a significant viscosity increase in the lower mantle is required to stabilize the large scale pattern of convection and bring TPW rates closer to observed values. *Richards et al.* [1999] find occasional inertial interchanges of polar axes with a duration of 20 Myr, due to avalanching in the lower mantle (though only one such event occurs in a 600 Myr numerical run).

[62] None of these early models actually feature lithospheric plates. The more recent study of M. Greff-Lefftz and P. Bunge (personal communication, 2000) and *Greff-Lefftz* [2001] explores the respective and cumulative effects of lower mantle viscosity, upper to lower mantle phase transitions and heat flux from the core on TPW estimates, combining 3-D spherical mantle circulation models with solutions to the equations of conservation of angular momentum. M. Greff-Lefftz and P. Bunge (personal communication, 2000) and *Greff-Lefftz* [2001] confirm that isoviscous mantle convection models predict TPW rates going from 100 km/Myr (the maximum acceptable value according to our study, applying to the current period) to 1000 km/Myr and more (i.e., unacceptable values for us, as long as the elusive superfast episodes are not confirmed). Greff-Lefftz and Bunge find that phase transitions have little effect, and that combination of very high lower mantle viscosity (100 times that of the upper mantle, identical to the average they use for the lithosphere) with 12% bottom heating from the core [*Davies*, 1988] results in calculated TPW closest to that which we observe. ''Because the rotation axis can only change as fast at the Earth's rotational bulge relaxes by means of viscous flow,'' inertial interchange almost never happens. However, M. Greff-Lefftz and P. Bunge (personal communication, 2000) and *Greff-Lefftz* [2001] insist that their models strongly underestimate the true vigor of mantle convection, hence strongly underestimate TPW rates.

[63] Therefore, all current modeling still fails to some (sometimes large) extent to account for the slow values of typical TPW velocity (30–100 km/Myr), and even more so to account for the prolonged ($\sim$50 Ma) periods with almost no TPW (standstills). Also they predict rather smooth evolutions, rather than the alternating episodes which we feel we uncover from the data. The remarkable similarity between TPW estimates for the Pacific plate and the rest of the world, which are based on completely different and independent data sets, lends support to the idea that significant TPW, on the order of 10° or more, occurred since before the Cretaceous. The importance of the Pacific plate and severe limitations on presently available data from that plate point to the need for many more direct (paleomagnetic core) measurements as opposed to indirect/remote sensing determinations of magnetization direction (i.e., ''skewness'' or ''seamount'' data). The possible links between episodes, or major changes between TPW episodes, and either plate motion and plate boundary reorganizations or avalanches, plumes and other major geodynamical events occurring in the lower mantle should remain the topic of fascinating, ongoing studies.

[64] **Acknowledgments.** Most computations, data handling and production of diagrams were made using the Paleomac software package

kindly provided by J. P. Cogné http://www.ipgp.jussieu.fr./~cogne). Part of this project was funded by INSU-CNRS Intérieur de la Terre (INSU-IT). We thank Stuart Gilder for comments, Randy Enkin and John Tarduno for very careful and useful reviews, and Ted Evans for efficient suggestions as Associate Editor. IPGP contribution NS 1759.

References

Acton, G. D., and R. G. Gordon, Paleomagnetic tests of Pacific plate reconstructions and implications for motion between hotspots, *Science*, *263*, 1246–1254, 1994.

Andrews, J. A., True polar wander: An analysis of Cenozoic and Mesozoic paleomagnetic poles, *J. Geophys. Res.*, *90*, 7737–7750, 1985.

Besse, J., Cinématique des plaques et dérive des pôles magnétiques: Evolution de la Téthys, collisions continentales et couplage manteau/noyau, thèse d'etat, 380 pp., Univ. Paris 7, Paris, France, 1986.

Besse, J., and V. Courtillot, Paleogeographic maps of the Indian Ocean bordering continents since the Upper Jurassic, *J. Geophys. Res.*, *93*, 11,791–11,808, 1988.

Besse, J., and V. Courtillot, Revised and synthetic polar wander paths of the African, Eurasian, North American, and Indian plates and true polar wander since 200 Ma, *J. Geophys. Res.*, *96*, 4029–4050, 1991.

Briden, J. C., Recurrent continental drift of Gondwanaland, *Nature*, *215*, 1334–1339, 1967.

Bullard, E. C., J. E. Everett, and A. G. Smith, A symposium on continental drift, IV, The fit of the continents around the Atlantic, *Philos. Trans. R. Soc. London*, *258*, 41–51, 1965.

Bunge, H.-P., M. A. Richards, C. Lithgow-Bertelloni, B. A. Romanowicz, and S. P. Grand, Time scales and heterogeneous structure in geodynamic Earth models, *Science*, *280*, 91–95, 1998.

Camps, P., M. Prévot, M. Daignières, and P. Machetel, Comment on "Stability of the Earth with respect to the spin axis for the last 130 million years" by J. A. Tarduno and A. Y. Smirnov, *Earth Planet. Sci. Lett.*, *198*, 529–532, 2001.

Cande, S., A paleomagnetic pole from the late Cretaceous marine magnetic anomalies in the Pacific, *Geophys. J. R. Astron. Soc.*, *44*, 547–566, 1976.

Carlut, J., and V. Courtillot, How complex is the time-averaged geomagnetic field over the past 5 Myr?, *Geophys. J. Int.*, *134*, 527–544, 1998.

Celaya, M. A., and B. M. Clement, Inclination shallowing in deep sea sediments from the North Atlantic, *Geophys. Res. Lett.*, *15*, 52–55, 1988.

Clouard, V., and A. Bonneville, How many Pacific hotspots are fed by deep mantle plumes?, *Geology*, *29*, 695–698, 2001.

Cogné, J. P., N. Halim, Y. Chen, and V. Courtillot, Resolving the problem of shallow magnetizations of Tertiary age in Asia: Insights from paleomagnetic data from the Qiangtang, Kunlun, and Qaidam blocks (Tibet, China), and a new hypothesis, *J. Geophys Res.*, *104*, 17,715–17,734, 1999.

Constable, C. G., and R. L. Parker, Statistics of the geomagnetic secular variation for the past 5 Myr, *J. Geophys. Res.*, *93*, 11,569–11,581, 1988.

Cottrell, R. D., and J. A. Tarduno, Late Cretaceous true polar wander: Not so fast, *Science*, *288*, 2283a, 2000.

Coupland, D. H., and R. Van der Voo, Long-term nondipole components in the geomagnetic field during the last 130 Ma, *J. Geophys. Res.*, *85*, 3529–3548, 1980.

Courtillot, V., J. Besse, and H. Théveniaut, North American Jurassic apparent polar wander: The answer from other continents?, *Phys. Earth Planet. Inter.*, *82*, 87–104, 1994.

Cox, A., and R. G. Gordon, Paleolatitudes determined from paleomagnetic data from vertical cores, *Rev. Geophys.*, *22*, 47–72, 1984.

Cox, A., and B. Hart, *Plate Tectonics: How It Works*, 392 pp., Blackwell Sci., Malden, Mass., 1986.

Davies, G. F., Ocean bathymetry and mantle convection, 1, Large-scale flow and hot spots, *J. Geophys. Res.*, *93*, 10,467–10,480, 1988.

Di Venere, V., and D. V. Kent, Are the Pacific and Indo-Atlantic hotspots fixed? Testing the plate circuit through Antarctica, *Earth Planet. Sci. Lett.*, *170*, 105–117, 1999.

Dyment, J., S. C. Cande, and J. Arkani-Hamed, Skewness of marine magnetic anomalies created between 85 and 40 Ma in the Indian Ocean, *J. Geophys. Res.*, *99*, 24,121–24,134, 1994.

Engebretson, D. C., A. Cox, and R. G. Gordon, Relative motions between oceanic and continental plates in the Pacific Basin, *Spec. Pap. Geol. Soc. Am.*, *206*, 59 pp., 1985.

Enkin, R. J., and G. S. Watson, Statistical analysis of paleomagnetic inclination data, *J. Geophys. Int.*, *126*, 495–504, 1996.

Enkin, R., Z. Yang, Y. Chen, and V. Courtillot, Paleomagnetic constraints on the geodynamic history of the major blocks of China from the Permian to the present, *J. Geophys. Res.*, *97*, 13,953–13,989, 1992.

Evans, D. A., True polar wander, a supercontinental legacy, *Earth Planet. Sci. Lett.*, *157*, 1–8, 1998.

Gordon, R., Late Cretaceous apparent polar wander of the Pacific plate: Evidence for a rapid shift of the Pacific hotspots with respect to spin axis, *Geophys. Res. Lett.*, *10*, 709–712, 1983.

Gordon, R., and A. Cox, Calculating paleomagnetic poles for oceanic plates, *Geophys. J. R. Astron. Soc.*, *63*, 619–640, 1980.

Greff-Lefftz, M., Déformation et rotation de la Terre, Mémoire d'habilitation, 120 pp., Univ. Paris 7, Paris, 2001.

Hargraves, R. B., Paleomagnetism of Mesozoic kimberlites in southern Africa and the Cretaceous apparent polar wander curve for Africa, *J. Geophys. Res.*, *94*, 1851–1866, 1989.

Harland, W. B., R. Armstrong, A. Cox, L. Craig, A. Smith, and D. Smith, *A Geologic Time Scale*, 263 pp., Cambridge Univ. Press, New York, 1989.

Hulot, G., M. Le Huy, and J. L. Le Mouël, Influence of core flows on the decade variations of the polar motion, *Geophys. Astrophys. Fluid Dyn.*, *82*, 35–67, 1996.

Irving, E., and G. A. Irving, Apparent polar wander paths: Carboniferous through Cenozoic and the assembly of Gondwana, *Geophys. Surv.*, *5*, 141–188, 1982.

Jaeger, J. J., V. Courtillot, and P. Tapponnier, Paleontological view of the ages of the Deccan traps, the Cretaceous/Tertiary boundary, and the India-Asia collision, *Geology*, *17*, 316–319, 1989.

Johnson, C., and C. G. Constable, The time-averaged geomagnetic field: Global and regional databases for 0–5 Ma, *Geophys. J. Int.*, *131*, 643–666, 1997.

Kent, D. V., and F. M. Gradstein, A Jurassic to recent chronology, in *The Geology of North America*, vol. M, *The Western Atlantic Region*, edited by P. R. Vogt and B. E. Tucholke, pp. 45–50, Geol. Soc. of Am., Boulder, Colo., 1986.

Koppers, A. A. P., J. P. Morgan, J. W. Morgan, and H. Staudigel, Testing the fixity of hot spots hypothesis using $^{40}Ar/^{39}Ar$ age progression along seamount trail, *Earth Planet Sci. Lett.*, *185*, 237–252, 2001.

Lawver, L. A., and C. Scotese, A revised reconstruction of Gondwanaland, in *Gondwana Six, Structure, Tectonics and Geophysics, Geophys. Monogr. Ser.*, vol. 40, edited by G. D. McKenzie, pp. 17–23, AGU, Washington, D. C., 1987.

Le Pichon, X., and J. M. Gaulier, The rotation of Arabia and the Levant fault system, *Tectonophysics*, *153*, 271–274, 1988.

Livermore, R. A., F. J. Vine, and A. G. Smith, Plate motions and the geomagnetic field, I, Quaternary and late Tertiary, *Geophys. J. R. Astron. Soc.*, *73*, 153–171, 1983.

Livermore, R. A., F. J. Vine, and A. G. Smith, Plate motions and the geomagnetic field, II, Jurassic to Tertiary, *Geophys. J. R. Astron. Soc.*, *79*, 939–961, 1984.

Machetel, P., and P. Weber, Intermittent layered convection in a model mantle with an endothermic phase change at 670 km, *Nature*, *350*, 55–57, 1991.

May, S. R., and R. Butler, North American Jurassic apparent polar wander: Implications for plate motion, paleogeography, and cordilleran tectonics, *J. Geophys. Res.*, *91*, 11,519–11,544, 1986.

McElhinny, M. W., and J. Lock, Four IAGA databases released in one package, *Eos Trans. AGU*, *76*, 266, 1995.

McElhinny, M. W., P. L. McFadden, and R. T. Merrill, The time averaged paleomagnetic field 0–5 Ma, *J. Geophys. Res.*, *101*, 25,007–25,027, 1996.

McFadden, P. L., and M. W. McElhinny, The combined analysis of remagnetization circle and direct observation in paleomagnetism, *Earth Planet. Sci. Lett.*, *87*, 161–172, 1988.

McFadden, P. L., and M. W. McElhinny, Classification of the reversal test in paleomagnetism, *Geophys. J. Int.*, *103*, 725–729, 1990.

Merrill, R. T., and M. W. McElhinny, *The Earth's Magnetic Field*, 401 pp., Academic, San Diego, Calif., 1983.

Molnar, P., and T. Atwater, Relative motion of hot spots in the mantle, *Nature*, *246*, 288–291, 1973.

Molnar, P., and J. Stock, Relative motions of hotspots in the Pacific, Atlantic and Indian Oceans since late Cretaceous time, *Nature*, *327*, 587–591, 1987.

Morgan, W. J., Hotspot tracks and the early rifting of the Atlantic, *Tectonophysics*, *94*, 123–139, 1983.

Müller, R. D., and W. R. Roest, Fracture zones in the North Atlantic from combined Geosat and Seasat data, *J. Geophys. Res.*, *97*, 3337–3350, 1992.

Müller, D. M., J. Y. Royer, and L. A. Lawver, Revised plate motions relative to the hotspots from combined Atlantic and Indian Ocean hotspot tracks, *Geology*, *21*, 275–278, 1993.

Norton, I. O., Plate motion in the North Pacific: The 43 Ma nonevent, *Tectonics*, *14*, 1080–1094, 1995.

Nürnberg, D., and R. D. Müller, The tectonic evolution of the South Atlantic from Late Jurassic to Present, *Tectonophysics*, *191*, 27–53, 1991.

Parker, R. L., A theory of ideal bodies for seamount magnetism, *J. Geophys. Res.*, *96*, 16,101–16,112, 1991.

Parker, R. L., L. Shure, and L. A. Hildebrand, The application of inverse theory to seamount magnetism, *Rev. Geophys.*, *25*, 17–40, 1987.

Patriat, P., and J. Achache, India-Eurasia collision chronology has implications for crustal shortening and driving mechanism of plates, *Nature*, *311*, 615–621, 1984.

Peirce, J. W., Assessing the reliability of DSDP paleolatitudes, *J. Geophys. Res.*, *81*, 4173–4187, 1976.

Peirce, J. W., The northward motion of India since the Late Cretaceous, *Geophys. J. R. Astron. Soc.*, *52*, 277–311, 1978.

Petronotis, K. E., and R. G. Gordon, A Maastrichtian paleomagnetic pole for the Pacific plate from a skewness analysis of marine magnetic anomaly 32, *Geophys. J. Int.*, *139*, 227–247, 1999.

Petronotis, K. E., R. G. Gordon, and G. D. Acton, Determining paleomagnetic poles and anomalous skewness from marine magnetic anomaly skewness data from a single plate, *Geophys. J. Int.*, *109*, 209–224, 1992.

Prévot, M., E. Mattern, P. Camps, and M. Daignières, Evidence for a 20° tilting of the Earth's rotation axis 110 million years ago, *Earth Planet. Sci. Lett.*, *179*, 517–528, 2000.

Quidelleur, X., J. P. Valet, V. Courtillot, and G. Hulot, Long-term geometry of the geomagnetic field for the last five million years: An updated secular variation database, *Geophys. Res. Lett.*, *21*, 1639–1642, 1994.

Ricard, Y., M. Richards, and Y. A. Le Stunff, A geodynamical model of mantle density heterogeneity, *J. Geophys. Res.*, *98*, 21,895–21,909, 1993.

Richards, M., H. P. Bunge, Y. Ricard, and J. R. Baumgardner, Polar wandering in model convections models, *Geophys. Res. Lett.*, *26*, 1777–1780, 1999.

Royer, J.-Y., and D. T. Sandwell, Evolution of the eastern India Ocean since the Late Cretaceous: Constraints from Geosat altimetry, *J. Geophys. Res.*, *94*, 13,755–13,782, 1989.

Royer, J.-Y., P. Patriat, H. Bergh, and C. R. Scotese, Evolution of the Southwest Indian Ridge from the Late Cretaceous (anomaly 34) to the middle Eocene (anomaly 20), *Tectonophysics*, *155*, 235–260, 1988.

Royer, J. Y., R. D. Müller, L. M. Gahagan, L. A. Lawver, C. L. Mayes, D. Nürnberg, and J. G. Sclater, A global isochron chart, *Tech. Rep. 117*, Univ. of Tex. Inst. for Geophys., Austin, 1992.

Sager, W. W., and A. A. P. Koppers, Late Cretaceous polar wander of the Pacific plate: Evidence of a rapid true polar wander event, *Science*, *287*, 455–459, 2000.

Sager, W. W., and S. Pringle, Mid Cretaceous to Early Tertiary apparent polar wander path of the Pacific plate, *J. Geophys. Res.*, *93*, 11,753–11,771, 1988.

Saunders, A. D., J. G. Fitton, A. C. Kerr, M. J. Norry, and R. W. Kent, The North Atlantic igneous province, in *Large Igneous Provinces, Geophys. Monogr. Ser.*, vol. 100, edited by J. J. Mahoney and M. F. Coffin, pp. 45–93, AGU, Washington, D.C., 1997.

Schneider, D. A., and D. V. Kent, The paleomagnetic field from equatorial deep sea sediments: Axial symmetry and polarity asymmetry, *Science*, *242*, 252–256, 1988.

Schneider, D. A., and D. V. Kent, Paleomagnetism of Leg 115 sediments: Implications for Neogene magnetostratigraphy and paleolatitude of the Reunion Hotspot, *Proc. Ocean Drill. Program Sci. Results*, *115*, 717–736, 1990a.

Schneider, D. A., and D. V. Kent, The time-averaged paleomagnetic field, *Rev. Geophys.*, *28*, 71–96, 1990b.

Schouten, H., and S. C. Cande, Palaeomagnetic poles from marine magnetic anomalies, *Geophys. J. R. Astron. Soc.*, *44*, 567–575, 1976.

Schouten, H., and K. McCamy, Filtering marine magnetic anomalies, *J. Geophys. Res.*, *77*, 7089–7099, 1972.

Srivastava, S. P., and C. R. Tapscott, Plate kinematics of the North Atlantic, in *The Geology of North America*, vol. M, *The Western Atlantic Region*, edited by B. E. Tucholke and P. R. Vogt, pp. 379–404, Geol. Soc. of Am., Boulder, Colo., 1986.

Steinberger, B., and R. J. O'Connell, Changes of the Earth's rotation axis owing to advection of mantle density heterogeneities, *Nature*, *387*, 169–173, 1997.

Steinberger, B., and R. J. O'Connell, Advection of plumes in mantle flow: Implications on hotspot motion, mantle viscosity and plume distribution, *Geophys. J. Int.*, *132*, 412–434, 1998.

Tackley, P., Mantle convection and plate tectonics: Toward an integrated physical and chemical theory, *Science*, *288*, 2002–2007, 2000.

Tackley, P. J., D. J. Stevenson, G. A. Glatzmaier, and G. Schubert, Effects of multiple phase-transitions in a three-dimensional spherical model of convection in Earth's mantle, *J. Geophys. Res.*, *99*, 15,877–15,901, 1994.

Tarduno, J. A., Absolute inclination values from deep sea sediments: A reexamination of the Cretaceous Pacific record, *Geophys. Res. Lett.*, *17*, 101–104, 1990.

Tarduno, J. A., and R. D. Cottrell, Paleomagnetic evidence for motion of the Hawaiian hotspot during formation of the Emperor Seamounts, *Earth Planet. Sci. Lett.*, *153*, 171–180, 1997.

Tarduno, J. A., and J. Gee, Large-scale motion between Pacific and Atlantic hotspots, *Nature*, *378*, 477–480, 1995.

Tarduno, J. A., and A. Y. Smirnov, Stability of the Earth with respect to the spin axis for the last 130 million years, *Earth Planet. Sci. Lett.*, *184*, 549–553, 2001.

Tauxe, L., P. Tucker, N. Petersen, and J. L. LaBrecque, The magnetostratigraphy of Leg 73 sediments, *Paleogeogr. Paleoclimatol. Paleoecol.*, *42*, 65–90, 1983.

Torcq, F., Evolution et destruction de la Pangée du Carbonifère au Jurassique, thèse de doctorat, 183 pp., Univ. Paris 7, Paris, France, 1997.

Vandamme, D., and V. Courtillot, Palaeomagnetism of Leg 115 basement rocks and latitudinal evolution of the Réunion hotspot, *Proc. Ocean Drill. Program Sci. Results*, *115*, 111–117, 1990.

Vandamme, D., V. Courtillot, J. Besse, and R. Montigny, Paleomagnetism and age determinations of the Deccan traps (India): Results of a Nagpur-Bombay traverse and review of earlier work, *Rev. Geophys.*, *29*, 159–190, 1991.

Van der Voo, R., Phanerozoic paleomagnetic poles from Europe and North America and comparisons with continental reconstructions, *Rev. Geophys.*, *28*, 167–206, 1990.

Van der Voo, R., *Paleomagnetism of the Atlantic, Tethys and Iapetus Oceans*, 411 pp., Cambridge Univ. Press, New York, 1993.

Westphal, M., M. L. Bazhenov, J. P. Lauer, D. M. Pechersky, and J. C. Sibuet, Paleomagnetic implications on the evolution of the Tethys belt from the Atlantic Ocean to the Pamirs since the Triassic, *Tectonophysics*, *123*, 37–82, 1986.

Wilson, R. L., Permanent aspects of the Earth's non-dipole magnetic field over Upper Tertiary times, *Geophys. J. R. Astron. Soc.*, *19*, 417–437, 1970.

Yang, Y., and J. Besse, New Mesozoic apparent polar wandering path for south China: Tectonic consequences, *J. Geophys. Res.*, *106*, 8493–8520, 2001.

J. Besse and V. Courtillot, Laboratoire de Paléomagnétisme, UMR 7577, Institut de Physique du Globe de Paris, 4 Place Jussieu, F-75252 Paris cedex 05, France. (besse@ipgp.jussieu.fr; courtil@ipgp.jussieu.fr)